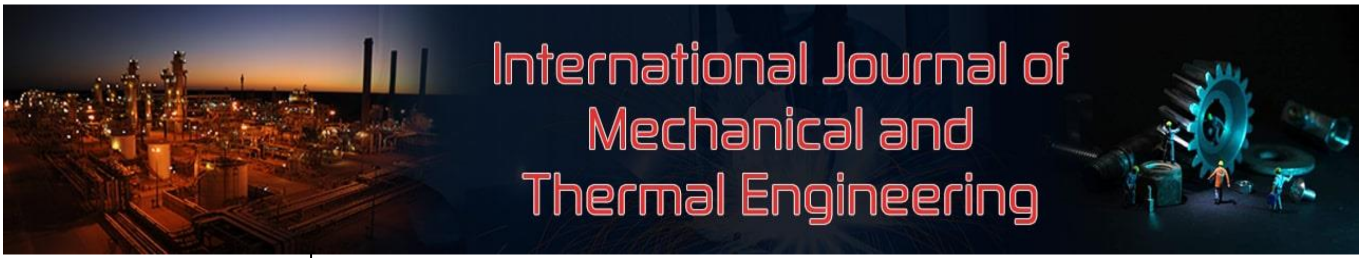

E-ISSN: 2707-8051
P-ISSN: 2707-8043
Impact Factor (RJIF): 5.89
IJMTE 202; 6(2): 65-92
www.mechanicaljournals.com/ijmte
Received: 24-06-2025
Accepted: 28-07-2025

Dr. Rajesh Patra
Associate Professor,
Department of Basic Science and Humanities Mathematics,
Hooghly Engineering & Technology College,
Vivekananda Road, Hooghly,
West Bengal India

Corresponding Author:
Dr. Rajesh Patra
Associate Professor,
Department of Basic Science and Humanities Mathematics,
Hooghly Engineering & Technology College,
Vivekananda Road, Hooghly,
West Bengal India

Nonhomogeneous thermo-mechanical analysis of a crack in an infinite functionally graded elastic layer

Rajesh Patra

DOI: https://www.doi.org/10.22271/27078043.2025.v6.i2a.98

Abstract
This study develops a steady-state thermoelastic solution for an infinite functionally graded material (FGM) layer of finite thickness containing a crack at its mid-plane, parallel to the surfaces. The layer is subjected to constant but unequal surface temperatures and symmetric concentrated forces of magnitude P/2, which may be tensile or compressive. Using the integral transform method, the problem is reduced to a Cauchy-type singular integral equation and solved numerically. Key results include the normalized thermo-mechanical stress intensity factor (TMSIF), thermal stress intensity factor (TSIF), and crack opening displacement, with graphical analysis showing how thermal loading and material gradation affect fracture behavior.

Keywords: Functionally graded materials, fracture mechanics, Fourier integral transform, singular integral equation, stress-intensity factor, crack opening displacement

1. Introduction
Every solid material has unique physical and mechanical properties such as elasticity, density, porosity, and conductivity that determine its suitability for specific applications. However, a single material often cannot me*et al*l the performance demands of complex environments. For instance, aerospace applications require materials that are lightweight, strong, and thermally insulating properties rarely found together in one material. Strong materials are typically heavy, while good insulators lack strength. To address this, engineers develop composite materials by combining different substances, each contributing specific advantages. This enables the creation of materials with customized properties suited for high-performance applications like aerospace, automotive, and construction.

Composite, fiber-reinforced, and functionally graded materials (FGMs) are modern materials used across various applications. FGMs are formed by gradually blending two materials, A and B, with properties varying spatially as a weighted mix-(100 - x) % of A and x % of B where $0 \leq x \leq 100$. Originating in Japan in the 1980s, FGMs offer advantages like corrosion resistance, thermal control, and improved strength, and are also widely used in biomedical engineering.

Thermal loading significantly influences the post-loading behavior of solids and must therefore be addressed with great care. Consequently, the study of thermoelastic problems has long been a vital area within solid mechanics (Nowacki [1], Nowinski [2], Boley and Weiner [3]). In structural engineering design, careful consideration of thermal stresses is essential, as many structural components are exposed to intense thermal environments. Such exposure can induce substantial thermal stresses, particularly in the vicinity of existing defects within the material. When combined with mechanical loads, these thermal stresses can lead to stress concentrations around defects, potentially resulting in serious structural damage.

Numerous earlier studies have contributed to the understanding of crack-related problems in solids. Important contributions include the works by Dag *et al.* [4, 5], Sherief and El-Mahraby [6], Chaudhuri and Ray [7, 8], Patra *et al.* [9, 10, 11], Rokhi and Shariati [12], Eskandari [13], Lee [14], among others. In addition, several recent investigations have continued to explore the behavior of cracks in solids, particularly in complex or functionally graded materials. Notable among these are the works of Kanaun [15], Barik *et al.* [16], Birinci *et al.* [17], Rekik *et al.* [18], Chen and Hu [19], Chang and Wang [20], Markov and Kanaun [21], Ding *et al.* [22], Wang *et al.* [23], which offer valuable insights into the theoretical and computational modeling of crack propagation and its effects on material performance.

In fracture mechanics, accurately determining the Stress Intensity Factor (SIF) is vital for assessing crack behavior under mechanical or thermal loading, as it measures stress concentration at crack tips. This is critical for designing fracture-resistant materials in structures like bridges, aircraft, and precision components. In thermoelastic problems, the Thermal Stress Intensity Factor (TSIF) is especially important, and has been widely studied for its role in thermal stress concentration. Noteworthy contributions in this area include the works of Ding and Li [24], Lee and Park [25], Itou [26], Liu and Kardomateas [27], Hosseini-Tehrani *et al*. [28], Nabavi and Shahani [29], Sur and Kanoria [30], Chen [31], among others.

The present investigation aims to find the steady-state thermoelastic solution for an infinite functionally graded material (FGM) layer of finite thickness containing a crack located at the mid-plane, parallel to the layer surfaces maintaining at constant unequal temperatures under steady state thermal loading as well as mechanical loading. The governing equations are reduced to a Cauchy-type singular integral equation, which is subsequently solved numerically. Key quantities of interest, including the normalized thermo-mechanical stress intensity factor (TMSIF), thermal stress intensity factor (TSIF), and the normalized crack opening displacement, are evaluated. The influence of nonhomogeneous thermal loading and material gradation parameters on these quantities is illustrated through graphical results, highlighting the effects of thermal and material non-homogeneity on the fracture behavior of the FGM layer.

2. Nomenclature

λ, μ	: Lame's constants for isotropic elastic material
ν	: Poisson's ratio of elastic material
α_t	: Thermal expansion coefficient of the material
$\sigma_x, \tau_{xy}, \sigma_y$	: Stress components in cartesian co-ordinate system
κ	: Thermal diffusivity of the material
P	: Applied load in isothermal problem
$\delta_1(:)$	: Dirac delta function
p_0	: Internal uniform pressure along crack surface
β	: Non-homogeneity parameter for elastic coefficients
$k(:)$	: Stress intensity factor in a medium with a crack in it
δ	: Non-homogeneity parameter for thermal coefficients
u, v	: Crack surface displacements
T	: Absolute temperature
T_0	: Reference temperature
T_1, T_2	: Constant temperature supplied to the material in the lower and
	upper region respectively

3. Formulation of the Problem

We consider an infinitely long functionally graded layer of thickness 2h weakened by the presence of an internal crack. Cartesian system co-ordinates will be used in our analysis. We shall take y-axis along the normal to the layer surface. The layer is infinite in a direction perpendicular to y-axis. A line crack of length 2b is assumed to be present in the middle of the layer. We shall take x-axis along the line of the crack with origin at the center of the crack and investigate the problem as a two-dimensional problem in the x-y plane. The crack faces are supposed to be acted upon by tensile force p_0 and the layer surfaces are acted upon by concentrated forces at points on the layer surfaces at distance 2a symmetrically positioned with respect to the center of the crack. The concentrated forces are either of compressive in nature or tensile in nature. Fig.1 displays the geometry of the problem.

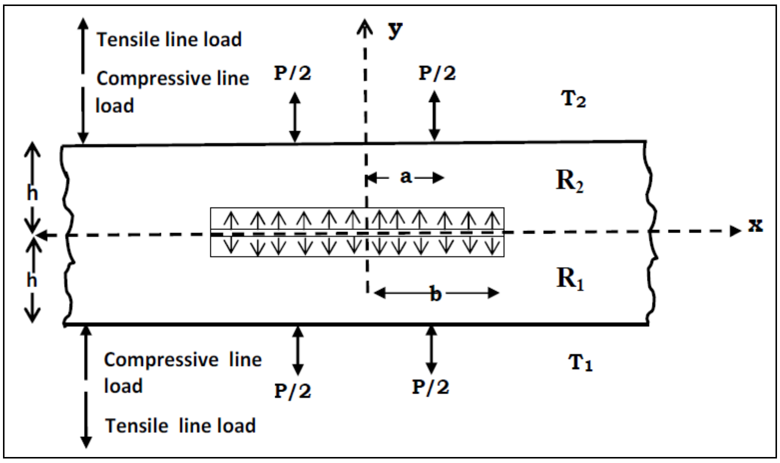

Fig 1: Geometry of the problem.

In this figure two sided arrows actually correspond to two distinct problems: the inward drawn arrows correspond to compressive loading, while outward drawn arrows correspond to tensile loading. The two different types of loading are (i) a pair of concentrated compressive loads each of magnitude $\frac{P}{2}$ applied symmetrically with respect to the center of the crack at a distance 2a apart, (ii) a pair of concentrated tensile loads each of magnitude $\frac{P}{2}$ applied symmetrically with respect to the center of the crack at a distance 2a apart. The gravitational force has not been taken into consideration. In deriving analytical solution in the present study, the thermo-mechanical properties dependent on the y-coordinate are modeled as exponential functions in the direction perpendicular to the plane of the crack, following the law

$$\kappa = \kappa_0 e^{\delta|y|}, \lambda = \lambda_0 e^{\beta|y|}, \mu = \mu_0 e^{\beta|y|}, \alpha = \alpha_t^0 e^{\gamma|y|}, \ (-h \le y \le h) \tag{1}$$

where κ_0, α_t^0 are the values of the heat conductivity and the thermal expansion coefficient with λ_0, μ_0, the elastic parameters in the homogeneous medium and β, the non-homogeneity parameter controlling the variation of the elastic parameters in the graded medium. Here, δ and γ are also non-homogeneity parameters. The strain displacement relations, linear stress-strain relations and equations of equilibrium are, respectively, given by

$$\varepsilon_x = \frac{\partial u}{\partial x}, \ \varepsilon_y = \frac{\partial v}{\partial y}, \gamma_{xy} = \frac{1}{2}\left(\frac{\partial u}{\partial y} + \frac{\partial v}{\partial x}\right), \tag{2}$$

$$\sigma_x = \frac{\mu}{\kappa-1}\left[(1+\kappa)\varepsilon_x + (3-\kappa)\varepsilon_y\right], \sigma_y = \frac{\mu}{\kappa-1}\left[(3-\kappa)\varepsilon_x + (1+\kappa)\varepsilon_y\right], \tag{3}$$

$$\frac{\partial \sigma_x}{\partial x} + \frac{\partial \tau_{xy}}{\partial y} = 0, \tag{4}$$

$$\frac{\partial \tau_{xy}}{\partial x} + \frac{\partial \sigma_y}{\partial y} = 0, \tag{5}$$

where $\kappa = 3 - 4\nu$ and ν is Poisson's ratio. Before further proceeding it will be convenient to adopt non-dimensional variables by rescaling all length variables by the problem's length scale b and the temperature variable by the reference temperature scale T_0:

$$u' = \frac{u}{b}, v' = \frac{v}{b}, x' = \frac{x}{b}, y' = \frac{y}{b}, h' = \frac{h}{b}, T' = \frac{T}{T_0}, T_1' = \frac{T_1}{T_0}, T_2' = \frac{T_2}{T_0}, \alpha_t' = \alpha_t T_0. \tag{6}$$

In the analysis below, for notational convenience, we shall use only dimensionless variables and shall ignore the dashes on the transformed non-dimensional variables. Mathematically, the problem under consideration is reduced to the solution of thermo-elasticity equations with thermal expansion coefficient α_t and the quantity H, the dimensionless thermal conductivity of the crack surface defined in Carslaw and Jaeger [32].

(i) Equilibrium equations

$$2(1-\nu)\frac{\partial^2 u}{\partial x^2} + (1-2\nu)\frac{\partial^2 u}{\partial y^2} + \frac{\partial^2 v}{\partial x \partial y} + \beta(1-2\nu)\left(\frac{\partial u}{\partial y} + \frac{\partial v}{\partial x}\right) = \beta_1 \frac{\partial T}{\partial x}, \tag{7}$$

$$(1-2\nu)\frac{\partial^2 v}{\partial x^2} + 2(1-\nu)\frac{\partial^2 v}{\partial y^2} + \frac{\partial^2 u}{\partial x \partial y} + \beta\left[2(1-\nu)\frac{\partial v}{\partial y} + 2\nu\frac{\partial u}{\partial x}\right] = \beta_1\left[\frac{\partial T}{\partial y} + (\beta+\gamma)T\right], \tag{8}$$

where $\beta_1 = 2(1+\nu)\alpha_t$.

(ii) Steady state heat conduction equation

$$\frac{\partial^2 T}{\partial x^2} + \frac{\partial^2 T}{\partial y^2} + \delta \frac{\partial T}{\partial y} = 0, \quad (0 < x < \infty), \tag{9}$$

(iii) The boundary conditions

(a) Thermal boundary conditions

$$T(x,-h) = T_1, \quad (0 < x < \infty) \tag{10}$$

$$T(x,h) = T_2, \quad (0 < x < \infty) \tag{11}$$

$$\frac{\partial}{\partial y} T(x,0^+) = \frac{\partial}{\partial y} T(x,0^-) = H[T(x,0^+) - T(x,0^-)], \quad (0 < x < 1) \tag{12}$$

$$T(x,0^+) = T(x,0^-), \quad (x \geq 1) \tag{13}$$

$$\frac{\partial}{\partial y} T(x,0^+) = \frac{\partial}{\partial y} T(x,0^-), \quad (x \geq 1) \tag{14}$$

(b) Elastic boundary conditions

$$\tau_{xy}(x,0) = 0, \quad (0 < x < \infty) \tag{15}$$

$$\tau_{xy}(x,h) = 0, \quad (0 < x < \infty) \tag{16}$$

$$\sigma_y(x,h) = \mp \frac{P}{2} \delta_1(x-a), \quad (0 < x < \infty) \tag{17}$$

$$\frac{\partial}{\partial x}[v(x,0)] = \begin{cases} f(x), & 0 < x < 1 \\ 0, & x > 1 \end{cases} \tag{18}$$

$$\sigma_y(x,0) = -p_0, \quad (0 \leq x \leq 1) \tag{19}$$

where u and v are the x and y components of the displacement vector; $\sigma_x, \sigma_y, \tau_{xy}$ are the normal and shearing stress components; $f(x)$ is an unknown function and $\delta_1(x)$ is the Dirac delta function. In Eq. (17) positive sign indicates tensile force while negative sign corresponds to compressive force.

4. Method of solution

a) Thermal part

To determine temperature field $T(x,y)$ from Eq. (9) and boundary conditions (10)-(14) we assume

$$T(x,y) = U(x,y) + W(y), \tag{20}$$

where $U(x,y)$ and $W(y)$ are two unknown functions satisfying the conditions

$$U(x,-h) = U(x,h) = 0, \tag{21}$$

$$W(-h) = T_1, W(h) = T_2. \tag{22}$$

Under these considerations we get

$$W(y)=\frac{T_1-T_2\,e^{2\delta h}}{1-e^{2\delta h}}y+\frac{T_2-T_1}{1-e^{2\delta h}}e^{-\delta(y-h)}, \tag{23}$$

$$U(x,y)=\begin{cases}\left[e^{m_1 y}-e^{(m_1-m_2)h+m_2 y}\right]A_1\,, & y\geq 0;\\ \left[e^{m_1 y}-e^{(m_2-m_1)h+m_2 y}\right]\frac{m_1-m_2e^{(m_1-m_2)h}}{m_1-m_2e^{-(m_1-m_2)h}}A_1\,, & y\leq 0.\end{cases} \tag{24}$$

where $m_1=\frac{1}{2}\left(-\delta+\sqrt{\delta^2+\eta^2}\right)$ and $m_2=\frac{1}{2}\left(-\delta-\sqrt{\delta^2+\eta^2}\right)$, (25)

for certain constants A_1 and η.
The appropriate temperature field satisfying the boundary conditions and regularity condition can be expressed as:

$$T(x,y)=\int_{-\infty}^{\infty}\left[e^{m_1 y}-e^{(m_1-m_2)h+m_2 y}\right]D(\eta)e^{-ix\eta}d\eta+W(y)$$

, for $y\ \geq\ 0$, (26)

$$T(x,y)=\int_{-\infty}^{\infty}\left[e^{m_1 y}-e^{(m_2-m_1)h+m_2 y}\right]r_{ab}D(\eta)e^{-ix\eta}d\eta+W(y)$$

, for $y\ \leq\ 0$ (27)

where $D(\eta)$ is an unknown function to be determined and

$$r_{ab}=\frac{m_1-m_2e^{(m_1-m_2)h}}{m_1-m_2e^{-(m_1-m_2)h}}\ . \tag{28}$$

Let us introduce the density function $\Theta(x)$, as

$$\Theta(x)=\frac{\partial}{\partial x}T(x,0^+)-\frac{\partial}{\partial x}T(x,0^-)\,, \tag{29}$$

It is clear from the boundary conditions (13) and (14) that

$\int_{-1}^{1}\Theta(x)dx=0\,,\quad (|x|<1)$ and (30)

$$\Theta(x)=0\,,\quad (|x|\ \geq 1). \tag{31}$$

Substituting Eq. (26) and (27) into Eq. (29) and using Fourier inverse transform, we Have

$$D(\eta)=\frac{i\left[m_1-m_2\,e^{-(m_1-m_2)h}\right]}{2\pi\eta(m_1-m_2)\left[e^{-(m_1-m_2)h}-e^{(m_1-m_2)h}\right]}\int_{-1}^{1}\Theta(s)e^{is\eta}ds\,, \tag{32}$$

Again, substituting Eq. (26) and (27) into Eq. (12) and applying the relation (32), we get the singular integral equation for $\Theta(s)$ as follows

$$\frac{1}{\pi}\int_{-1}^{1}\left[\frac{1}{s-x}+k_1(x,s)\right]\Theta(s)ds=\frac{\delta(T_2-T_1)e^{\delta h}}{1-e^{2\delta h}}\,,\quad (-1\ <x\ <1) \tag{33}$$

with

$$k_1(x,s) = \int_0^{\infty}\left[1-\frac{H}{\eta}+\frac{m_1^2+m_2^2-m_1m_2\left[e^{-(m_1-m_2)h}+e^{(m_1-m_2)h}\right]}{\eta(m_1-m_2)\left[e^{-(m_1-m_2)h}-e^{(m_1-m_2)h}\right]}\right]\sin\eta(x-s)\,d\eta\ . \tag{34}$$

After determining $\Theta(s)$ from the singular integral Eq. (33) we have the temperature field along the axes as

$$T(x,0) = \begin{cases} \dfrac{1}{\pi}\displaystyle\int_0^{\infty}\left[\frac{(m_1+m_2)-\left[m_1e^{-(m_1-m_2)h}+m_2e^{(m_1-m_2)h}\right]}{(m_1-m_2)\left[e^{-(m_1-m_2)h}-e^{(m_1-m_2)h}\right]}\times\frac{\sin\eta(x-s)}{\eta}\right]d\eta \\ \qquad \times\displaystyle\int_{-1}^{+1}\Theta(s)ds+\frac{(1-e^{\delta h})(T_1+T_2e^{\delta h})}{1-e^{2\delta h}}, \qquad (y\le 0) \\ \dfrac{1}{\pi}\displaystyle\int_0^{\infty}\left[\frac{(m_1+m_2)-\left[m_1e^{(m_1-m_2)h}+m_2e^{-(m_1-m_2)h}\right]}{(m_1-m_2)\left[e^{-(m_1-m_2)h}-e^{(m_1-m_2)h}\right]}\times\frac{\sin\eta(x-s)}{\eta}\right]d\eta \\ \qquad \times\displaystyle\int_{-1}^{+1}\Theta(s)ds+\frac{(1-e^{\delta h})(T_1+T_2e^{\delta h})}{1-e^{2\delta h}}, \qquad (y\ge 0) \end{cases} \tag{35}$$

$$T(0,y) = \begin{cases} \dfrac{1}{\pi}\displaystyle\int_0^{\infty}\frac{\left[e^{m_1y}-e^{-(m_1-m_2)h+m_2y}\right]\times\left[m_1^2+m_2^2-m_1m_2\left\{e^{-(m_1-m_2)h}+e^{(m_1-m_2)h}\right\}\right]}{(m_1-m_2)\left[e^{-(m_1-m_2)h}-e^{(m_1-m_2)h}\right]}d\eta \\ \qquad \times\displaystyle\int_{-1}^{+1}\Theta(s)\frac{\sin(\eta s)}{\eta}ds+W(y), \qquad (y\le 0) \\ \dfrac{1}{\pi}\displaystyle\int_0^{\infty}\frac{\left[e^{m_1y}-e^{(m_1+m_2)h+m_2y}\right]\times\left[m_1-m_2e^{-(m_1-m_2)h}\right]}{(m_1-m_2)\left[e^{-(m_1-m_2)h}-e^{(m_1-m_2)h}\right]}d\eta \\ \qquad \times\displaystyle\int_{-1}^{+1}\Theta(s)\frac{\sin(\eta s)}{\eta}ds+W(y), \qquad (y\ge 0) \end{cases} \tag{36}$$

where $W(y)$ is mentioned in Eq. (23).

(b) Elastic part

First of all, we observe that due to symmetry of the crack location with respect to the layer and of the applied load with respect to the crack, it is sufficient to consider the solution of the problem in the regions $0 \le x < \infty$ and $0 \le y \le h$. To solve the partial differential Eq. (7) and (8), Fourier transform is applied to the equations with respect to the variable x.
Utilizing the symmetric condition, the displacement components u, v may be written as

$$u(x,y) = \frac{2}{\pi}\int_0^{\infty}\Phi(\xi,y)\sin(\xi x)d\xi\ , \tag{37}$$

$$v(x,y) = \frac{2}{\pi}\int_0^{\infty}\Psi(\xi,y)\cos(\xi x)d\xi\ , \tag{38}$$

where $\Phi(\xi,y)$ and $\Psi(\xi,y)$ are Fourier transforms of $u(x,y)$ and $v(x,y)$, respectively with respect to the coordinate x, and ξ is the transformed parameter.
Substituting $u(x,y)$ and $v(x,y)$ from Eqs. (37) and (38) into the equations of equilibrium (7) and (8), we obtain the differential equation for the determination of $\Phi(\xi,y)$,

$$F(D_1)\Phi = -\frac{7-\kappa}{\kappa+1}\alpha_t\xi\,\frac{\partial^2 T_c}{\partial y^2}$$

$$+\frac{1}{2(\kappa+1)}\left[-\beta(\kappa+1)(7-\kappa)+\frac{(7-\kappa)\{4(\beta+\gamma)-(\kappa+1)^2(3-\kappa)\}}{\kappa^2-1}\right]\alpha_t\xi\,\frac{\partial\overline{T}_c}{\partial y}$$

$$+\frac{7-\kappa}{4(\kappa+1)^2}[(\kappa+1)\{4\xi^2+\beta^2(\kappa+1)(3-\kappa)\}+\beta\{4(\beta+\gamma)-(\kappa+1)^2(3-\kappa)\}]\alpha_t\xi\,\overline{T}_c, \text{ where} \tag{39}$$

$$F(D_1)=D_1^4+2\beta D_1^3-\left(2\xi^2-\beta^2\right)D_1^2-2\xi^2\beta D_1+\xi^2\left\{\xi^2-\frac{\kappa-3}{\kappa+1}\beta^2\right\},$$

with $D_1=\frac{\partial}{\partial y}$, (40)

and $\overline{T}_c(\xi,y)$ is the Fourier Cosine transform of $T(x,y)$ defined by

$$\overline{T}_c(\xi,y)=\int_0^\infty T(x,y)\cos(\xi x)\,dx. \tag{41}$$

The solution of the Eq. (39) is of the form

$$\Phi(\xi,y)=\sum_{i=1}^4\left[A_i(\xi)e^{t_i y}+f_i^{(j)}(\xi)\right],\ (j=1,2) \tag{42}$$

where $A_i(\xi),(i=1,\dots,4)$ are constants to be determined from the boundary conditions, $t_i(i=1,\dots,4)$ are the four complex roots of the quadratic equation

$$t^4+2\beta t^3-(2\xi^2-\beta^2)t^2-2\xi^2\beta t+\xi^2\left[\xi^2-\frac{\kappa-3}{\kappa+1}\beta^2\right]=0, \tag{43}$$

$$f_1^{(j)}(\xi)=\frac{1}{F(D_1)}\int_{-\infty}^{\infty}\left[-m_1^2\frac{7-\kappa}{\kappa+1}\alpha_t\xi+m_1\left\{-\frac{\beta(\kappa-1)(7-\kappa)}{2(\kappa+1)}+\frac{(7-\kappa)[4(\beta+\gamma)-(\kappa+1)^2(3-\kappa)]}{2(\kappa+1)^2(\kappa-1)}\right\}\alpha_t\xi\right.$$

$$\left.+\frac{7-\kappa}{4(\kappa+1)^2}\{(\kappa+1)[4\xi^2+\beta^2(\kappa+1)(3-\kappa)]+\beta[4(\beta+\gamma)-(\kappa+1)^2(3-\kappa)]\}\alpha_t\xi\right]$$
$$\times\frac{i\eta}{\xi^2-\eta^2}D(\eta)(r_{ab})^{(2-j)}e^{m_1 y}d\eta,\ (j=1,2) \tag{44}$$

$$f_2^{(j)}(\xi)=\frac{1}{F(D_1)}\int_{-\infty}^{\infty}\left[m_2^2\frac{7-\kappa}{\kappa+1}\alpha_t\xi-m_2\left\{-\frac{\beta(\kappa-1)(7-\kappa)}{2(\kappa+1)}+\frac{(7-\kappa)[4(\beta+\gamma)-(\kappa+1)^2(3-\kappa)]}{2(\kappa+1)^2(\kappa-1)}\right\}\alpha_t\xi\right.$$

$$\left.-\frac{7-\kappa}{4(\kappa+1)^2}\{(\kappa+1)[4\xi^2+\beta^2(\kappa+1)(3-\kappa)]+\beta[4(\beta+\gamma)-(\kappa+1)^2(3-\kappa)]\}\alpha_t\xi\right]$$

$$\times \frac{i\eta}{\xi^2-\eta^2} D(\eta)(r_{ab})^{(2-j)} e^{(-1)^j(m_1-m_2)h+m_2 y} d\eta, (j = 1,2)$$

(45)

$$f_3^{(j)}(\xi) = \frac{1}{F(D_1)}\left[-\frac{7-\kappa}{\kappa+1}\frac{\pi}{2}\frac{(T_2-T_1)\delta^2}{1-e^{2\delta h}}\alpha_t\xi\right.$$

$$-\left\{-\frac{\beta(\kappa-1)(7-\kappa)}{2(\kappa+1)} + \frac{(7-\kappa)[4(\beta+\gamma)-(\kappa+1)^2(3-\kappa)]}{2(\kappa+1)^2(\kappa-1)}\right\}\frac{\pi}{2}\frac{(T_2-T_1)\delta}{1-e^{2\delta h}}\alpha_t\xi$$

$$+\frac{7-\kappa}{4(\kappa+1)^2}\{(\kappa+1)[4\xi^2+\beta^2(\kappa+1)(3-\kappa)] + \beta[4(\beta+\gamma)-(\kappa+1)^2(3-\kappa)]\}\alpha_t\xi$$

$$\left.\times \frac{\pi}{2}\frac{(T_2-T_1)}{1-e^{2\delta h}}\right] e^{-\delta(y-h)}\delta_1(\xi), (j = 1,2)$$

(46)

$$f_4^{(j)}(\xi) = \frac{1}{F(D_1)}\frac{7-\kappa}{4(\kappa+1)}[(\kappa+1)\{4\xi^2+\beta^2(\kappa+1)(3-\kappa)\}\alpha_t\xi$$

$$+\beta\{4(\beta+\gamma)-(\kappa+1)^2(3-\kappa)\}] \times \frac{\pi}{2}\frac{(T_1-T_2e^{2\delta h})}{1-e^{2\delta h}}\delta_1(\xi), \ (j = 1,2)$$

(47)

where j=1,2 are for the lower (R_1) and upper (R_2) region respectively.

The function $\Psi(\xi,y)$ can then be determined as

$$\Psi(\xi,y) = \sum_{i=1}^{4}\left[M_i(\xi)A_i(\xi)e^{t_i y} + N_i f_i^{(j)}(\xi)\right], (j = 1,2)$$

with (48)

$$M_i(\xi) = \frac{(\kappa-1)t_i^2+\beta(\kappa-1)t_i-\xi^2(\kappa+1)}{\xi[2t_i+\beta(\kappa-1)]}, (i = 1,\dots,4),$$ (49)

$$N_i(\xi) = \frac{(\kappa-1)D_1^2+\beta(\kappa-1)D_1-\xi^2(\kappa+1)}{\xi[2t_i+\beta(\kappa-1)]}, (i = 1,\dots,4).$$ (50)

It follows from Eq. (43) that $t_3 = \overline{t_1}$ and $t_4 = \overline{t_2}$ where $\overline{(:)}$ represent complex conjugates with

$$t_1 = -\frac{\beta}{2} + \sqrt{\xi^2+\frac{\beta^2}{4}+i\xi\beta\sqrt{\frac{3-\kappa}{\kappa+1}}},$$ (51)

$$t_2 = -\frac{\beta}{2} - \sqrt{\xi^2+\frac{\beta^2}{4}+i\xi\beta\sqrt{\frac{3-\kappa}{\kappa+1}}}.$$ (52)

Substituting Eq. (37), (38) into Eq. (2) and (3) and utilizing Eq. (42) and (48) we obtain

$$\frac{1}{2\mu}\sigma_x(x,y) = \frac{2}{\pi}\int_0^{\infty}\frac{1}{2(1-\kappa)}\sum_{i=1}^{4}[\{-(1+\kappa)\xi - (3-\kappa)t_i M_i\}A_i e^{t_i y} + \left\{-\xi(1+\kappa)f_i^{(j)} - (3-\kappa)D_1\left(N_i f_i^{(j)}\right)\right\}]\cos(\xi x)d\xi\,,\ (j=1,2\,) \tag{53}$$

$$\frac{1}{2\mu}\sigma_y(x,y) = \frac{2}{\pi}\int_0^{\infty}\frac{1}{2(1-\kappa)}\sum_{i=1}^{4}[\{-(1+\kappa)t_i M_i - (3-\kappa)\xi\}A_i e^{t_i y} + \left\{-(1+\kappa)D_1\left(N_i f_i^{(j)}\right) - (3-\kappa)\xi f_i^{(j)}\right\}]\cos(\xi x)d\xi\,,\ (\,j=1,2) \tag{54}$$

$$\frac{1}{2\mu}\tau_{xy}(x,y) = \frac{2}{\pi}\int_0^{\infty}\sum_{i=1}^{4}\left[\left\{-\frac{\xi}{2}M_i + \frac{t_i}{2}\right\}A_i e^{t_i y} + \left\{-\frac{\xi}{2}N_i f_i^{(j)} + \frac{1}{2}D_1\left(f_i^{(j)}\right)\right\}\right]\sin(\xi x)d\xi\,,\quad (\,j=1,2) \tag{55}$$

From the boundary conditions (15)-(18), the unknown constants $A_i\ (i=1,\ldots,4)$ can be found out from the following linear algebraic system of equations expressed in matrix form:

$$LA = B\,, \tag{56}$$

where the matrices $L\,,\ A\,,\ B$ are

$$L = \begin{bmatrix} S_1 e^{t_1 h} & S_2 e^{t_2 h} & S_3 e^{t_3 h} & S_4 e^{t_4 h} \\ G_1 e^{t_1 h} & G_2 e^{t_2 h} & G_3 e^{t_3 h} & G_4 e^{t_4 h} \\ t_1 - G_1 & t_2 - G_2 & t_3 - G_3 & t_4 - G_4 \\ G_1 & G_2 & G_3 & G_4 \end{bmatrix},\quad A = \begin{bmatrix} A_1 \\ A_2 \\ A_3 \\ A_4 \end{bmatrix},\quad B = \begin{bmatrix} -R_1 - P_1 \\ P_2 \\ -R_2 - P_3 \\ P_4 \end{bmatrix}$$, with

$$R_1(\xi) = \pm\frac{(\kappa-1)}{2\mu}P[\cos(a\xi) + \cos(-a\xi)],\qquad R_2(\xi) = \int_0^{\infty} f(x)\sin(\xi x)dx\,,$$

$$P_1 = \sum_{i=1}^{4} D'_{4i} f_{ih}^{(j)}\,, P_2 = \sum_{i=1}^{4} D_{4i} f_{ih}^{(j)}\,,\ P_3 = \sum_{i=1}^{4} N_i f_{i0}^{(j)}\,,\ P_4 = \sum_{i=1}^{4} D_{4i} f_{i0}^{(j)}\,, (\,j=1,2) \tag{57}$$

$$S_i = (1+\kappa)t_i M_i + (3-\kappa)\xi\,,\quad G_i = -\xi M_i + t_i\,,\quad (i=1,\ldots\ldots,4). \tag{58}$$

$$D_{4i} = \xi\left[N_i - \frac{1}{\xi}D_1\right],\ \ D'_{4i} = (1+\kappa)D_1 N_i + (3-\kappa)\xi\,,\quad (\,i=1,\ldots\ldots,4\,). \tag{59}$$

Eq. (56) ayields

$$A_i(\xi) = D_{1i}(\xi)R_1(\xi) + D_{2i}(\xi)R_2(\xi) + D_{3i}(\xi), \quad (i = 1, \dots\dots, 4), \tag{60}$$

where $D_{ki}(\xi)(k = 1,2,3 \quad \text{and} \quad i = 1, \dots\dots, 4)$ are shown in **Appendix.** Substitution of these values into the Eq. (19) will lead to the following singular integral equation:

$$\frac{1}{\pi}\int_{-b}^{b} f(t)\left[\frac{1}{t-x} + k_2(x,t)\right]dt = \frac{(\kappa-1)}{\mu\chi}\left[-p_0 \pm \frac{P}{2\pi}k_3(x) + p_0 k_4(x)\right], (-b < x < b), \tag{61}$$

Where;

$$k_2(x,t) = \frac{1}{\chi}\int_0^\infty \sum_{i=1}^4 [D_{2i}S_i - \chi] \sin\xi(t-x)\,d\xi, \tag{62}$$

$$k_3(x) = -\int_0^\infty \sum_{i=1}^4 D_{1i}S_i[\cos\xi(a-x) + \cos\xi(a+x)]\,d\xi, \tag{63}$$

$$k_4(x) = -\frac{2\mu}{\pi p_0(\kappa-1)}\int_0^\infty \sum_{i=1}^4 \left[D_{3i}S_i - D'_{4i}f_{i0}^{(j)}\right]\cos(\xi x)\,d\xi, \quad (j = 1,2) \tag{64}$$

$$\chi = \lim_{\xi\to\infty} \sum_{i=1}^4 D_{2i}S_i = (3-\kappa). \tag{65}$$

The kernels $k_2(x,t)$ and $k_3(x)$, $k_4(x)$ are bounded and continuous in the closed interval $-b \le x \le b$. The integral equation must be solved under the following single valuedness condition

$$\int_{-b}^{b} f(t)\,dt = 0, \tag{66}$$

Before further proceeding it will be convenient to introduce non-dimensional variables r and s by rescaling all lengths in the problem by length scale b:

$$x = br, t = bs, \tag{67}$$

$$f(t) = f(bs) = \frac{p_0(\kappa-1)}{\mu\chi}\phi(s), \omega = \xi b, \tag{68}$$

In terms of non-dimensional variables, the integral Eq. (61) and single valuedness condition (66) becomes

$$\frac{1}{\pi}\int_{-1}^{1}\left[\frac{1}{s-r} + k_2^*(r,s)\right]\phi(s)\,ds = -1 \pm \frac{Q}{\pi}k_3^*(r) + k_4^*(r), (-1 < r < 1), \tag{69}$$

with

$$k_2^*(r,s) = \frac{1}{\chi}\int_0^\infty \left[\sum_{i=1}^4 D_{2i}S_i - \chi\right]\sin\omega(s-r)\,d\omega, \tag{70}$$

$$k_3^*(r) = -\int_0^\infty \sum_{i=1}^4 D_{1i}S_i[\cos\omega(a^*-r) + \cos\omega(a^*+r)]\,d\omega, \tag{71}$$

$$k_4^*(r) = -\frac{2\mu_0}{\pi p_0 b(\kappa-1)} \int_0^\infty \sum_{i=1}^4 \left[D_{3i} S_i - D'_{4i} f_{i0}^{(j)}\right] \cos(\omega r) d\omega \,, \ (j = 1,2) \tag{72}$$

$a^* = \frac{a}{b}$ and Q is the load ratio defined as: $Q = \frac{P}{2b\,p_0}$, (73)

$$f_{i0}^{(j)} \equiv f_i^{(j)}\Big|_{y=0}, \ f_{ih}^{(j)} \equiv f_i^{(j)}\Big|_{y=h}, \ (i = 1,2,3 \,; j = 1,2), D_1 \equiv \frac{\partial}{\partial y}. \tag{74}$$

5. Solution of The Integral Equations

a) Thermal part

The singular integral equation Eq. (33) is a Cauchy-type singular integral equation for an unknown function $\Theta(s)$. For the evaluation of thermal stress, it is necessary to solve the integral equation Eq. (33). For the purpose we write

$$\Theta(s) = \frac{\Upsilon(s)}{\sqrt{1-s^2}} \,, \ (-1 < s < 1) \,, \tag{75}$$

where $\Upsilon(s)$ is a regular and bounded unknown function. Substituting Eq. (75) into Eq. (33) and using Gauss-Chebyshev formula (Erdogan and Gupta [33]), we obtain

$$\frac{1}{N}\left[\sum_{k=1}^N \left\{\frac{1}{s_k - x_i} + k_1(x_i, s_k)\right\} \Upsilon(s_k)\right] = \frac{\delta(T_2 - T_1)e^{\delta h}}{1 - e^{2\delta h}} \,, \ (i = 1,2,\dots\dots\dots, N-1) \,, \tag{76}$$

$$\frac{\pi}{N}\sum_{k=1}^N \Upsilon(s_k) = 0 \,, \tag{77}$$

where s_k and x_i are given by

$$s_k = \cos\left(\frac{2k-1}{2N}\pi\right), (k = 1,2,3,\dots,N) \ \text{and} \ x_i = \cos\left(\frac{\pi i}{N}\right), (i = 1,2,3,\dots,N-1) \tag{78}$$

We observe that corresponding to $(N-1)$ collocation points $x_i = \cos\left[\frac{i\pi}{2(N+1)}\right]$, $i = 1,2,\dots\dots,(N-1)$, the Eq. (76) and (77) represent a set of N linear equations in N unknowns $\Upsilon(s_1), \Upsilon(s_2), \dots\dots\dots\dots\dots\dots, \Upsilon(s_N)$. This linear algebraic system of equations are solved numerically by utilizing Gaussian elimination method.

(b) Elastic part

The singular integral equation Eq. (69) is a Cauchy-type singular integral equation for an unknown function $\phi(s)$. Expressing now the solution of Eq. (69) in the form

$$\phi(s) = \frac{\psi(s)}{\sqrt{1-s^2}} \,, \ (-1 < s < 1) \,, \tag{79}$$

where $\psi(s)$ is a regular and bounded unknown function and using Gauss-Chebyshev formula (Erdogan and Gupta [33]), to evaluate the integral equation Eq. (69), we obtain,

$$\frac{1}{N}\left[\sum_{k=1}^N \left\{\frac{1}{s_k - r_i} + k_2^*(r_i, s_k)\right\} \psi(s_k)\right] = -1 \pm \frac{Q}{\pi} k_3^*(r_i) + k_4^*(r_i), \ (i = 1,2,..,N-1), \tag{80}$$

$$\frac{\pi}{N}\sum_{k=1}^{N}\psi(s_k)=0\,, \tag{81}$$

where r_i is given by

$$r_i=\cos\left(\frac{i\pi}{N}\right),\ (i=1,2,3,\dots\dots,N-1)\,. \tag{82}$$

We observe that corresponding to $(N-\ 1)$ collocation points $x_r=\cos\left[\frac{r\pi}{2(N+1)}\right]$, $r=1,2,\dots\dots,(N-1)$, the Eq. (80) and (81) represent a set of N linear equations in N unknowns $\psi(s_1),\psi(s_2),\dots\dots\dots\dots\dots\dots,\psi(s_N)$. This linear algebraic system of equations are solved numerically by utilizing Gaussian elimination method.

6. Determination of stress-intensity factor

The presence of a crack in a solid significantly alters the stress distribution compared to when no crack is present. Although the stress field remains largely undisturbed in regions far from the crack, the stresses near the crack tip become extremely high. To assess whether a crack is likely to propagate, fracture mechanics introduces a key physical quantity known as the stress intensity factor (SIF). In the problem at hand, the solid is subjected to two types of loading:(a) Thermal loading, (b) Mechanical loading - specifically, concentrated forces of magnitude $\frac{P}{2}$ applied symmetrically on the crack faces. The stress components $\sigma_x,\sigma_y,\tau_{xy}$, as given by Eq. (53) - (55), do not have closed-form solutions. Instead, they are represented as infinite integrals and must be evaluated numerically. In this discussion, we aim to determine two main quantities: the thermomechanical stress intensity factor (TMSIF), which reflects the combined effects of thermal and mechanical loading, and the thermal stress intensity factor (TSIF), which considers only thermal loading. The stress intensity factor is defined as follows:

$$k(b)=\lim_{r\to 1}\sqrt{2b(r-1)}\sigma_y^*(r,0).$$

The non-dimensional stress intensity factor (TMSIF), can be obtained in terms of the solution of the integral equation (69) as

$$\text{TMSIF}=k'(b)=\frac{1}{p_0\sqrt{b}}\lim_{r\to 1}\sqrt{2b(r-1)}\sigma_y^*(r,0)=-\psi(1), \tag{83}$$

When there is only thermal loading, the TSIF can be extracted following the same procedure as discussed above. In this case the Eq. (69) will be modified to

$$\frac{1}{\pi}\int_{-1}^{1}\left[\frac{1}{s-r}+k_2^*(r,s)\right]\phi(s)ds=-1+k_4^*(r)\,,(-1<r<1)\,, \tag{84}$$

The TSIF at the crack tip can be expressed based on the solution of integral equation (85) as follows:

$$\text{TSIF}=\frac{1}{p_0\sqrt{b}}\lim_{r\to 1}\sqrt{2b(r-1)}\sigma_y^*(r,0)=-\Omega(1), \tag{85}$$

In this case we assume

$$\phi(s)=\frac{\Omega(s)}{\sqrt{1-s^2}}\,,\ (-1<s<1), \tag{86}$$

where $\Omega(s)$ is regular and bounded unknown function and $\psi(1),\Omega(1)$ can be found out from $\psi(s_k)$ and $\Omega(s_k)$ $(k=1,2,3,\dots\dots\dots,N)$ using the interpolation formulas given by Krenk [34]. Following the method as in Gupta and Erdogan [35], we obtain the crack surface displacement (CSD) in the form

$$v'(r,0) = \int_{-1}^{r} \frac{\psi(s)}{\sqrt{1-s^2}} ds \,, \ (-1 < s < 1), \text{ with} \tag{87}$$

$$v'^{(r,0)} = \frac{v(r,0)}{b} \frac{\mu(3-\kappa)}{p_0(\kappa-1)}, \tag{88}$$

which can be obtained using Simpson's $\frac{1}{3}$ integration and appropriate interpolation formula.

7. Numerical results and discussions

This study investigates an internal crack in an infinite functionally graded layer under thermal effects, focusing on how temperature, grading parameters, and applied loads influence the stress intensity factor and crack opening displacement. Using a standard numerical method, the normal displacement and stress intensity factor are computed and presented graphically. Regions R_1 and R_2 refer to the areas below and above the crack line, respectively, and the non-homogeneity parameter γ is set to 0.1 for the analysis.

Fig. 2(a) illustrates the temperature distribution $T(x,0)$ along the crack face and its extension line for different values of the geometric parameter $\frac{b}{h}$, while keeping other parameters constant. The temperature profiles are symmetric about the crack center $x = 0$, as expected due to the problem's geometric and boundary condition symmetry. As the ratio $\frac{b}{h}$ increases, the temperature distribution becomes more pronounced, with deeper troughs and broader central regions. For a lower $\frac{b}{h}$ ratio, the temperature at the crack center is relatively high, and the minimum temperature along the crack face remains moderately elevated. In contrast, as the $\frac{b}{h}$, ratio increases, the maximum temperature at the center decreases, while the minimum temperature along the crack face drops significantly, indicating a sharper and more intensified thermal gradient. Fig. 2(b) and 2(c) illustrate the temperature distribution along the vertical centerline $x = 0$ for various values of the aspect ratio $\frac{b}{h}$, under fixed physical and thermal parameters. The results demonstrate that the temperature profile is significantly influenced by the variation in $\frac{b}{h}$. The temperature distribution along $x = 0$, taking $T_1 > T_2$, temperature decreases linearly both in the region R_1 and R_2. There is one point to note here that the variations of temperature at a particular point on $x = 0$ below and above the line of crack are opposite in nature in respect of the values of $\frac{b}{h}$. An increase in $\frac{b}{h}$ leads to a steeper temperature gradient along the y-axis, particularly near the domain boundaries, indicating enhanced thermal conduction effects.

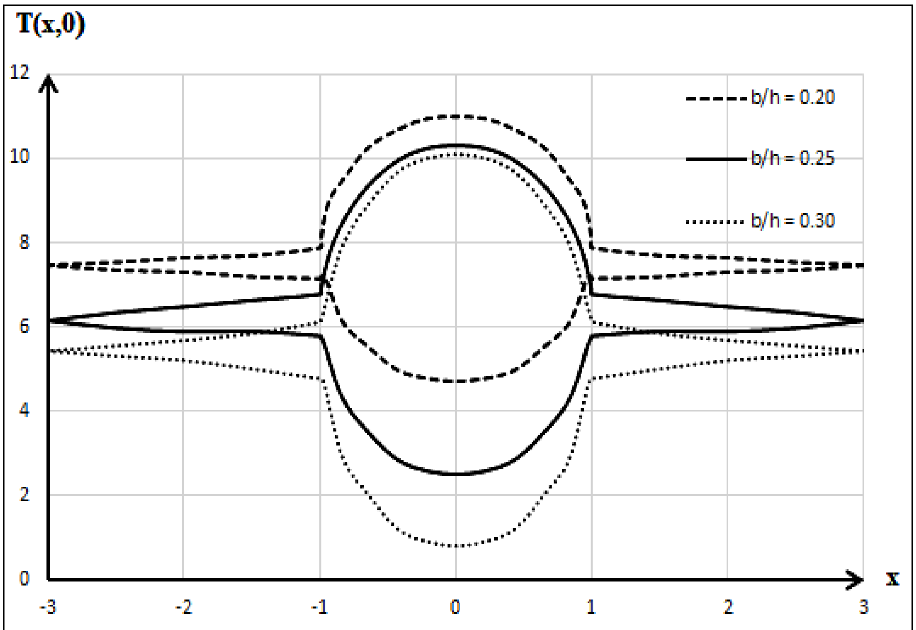

2(a)

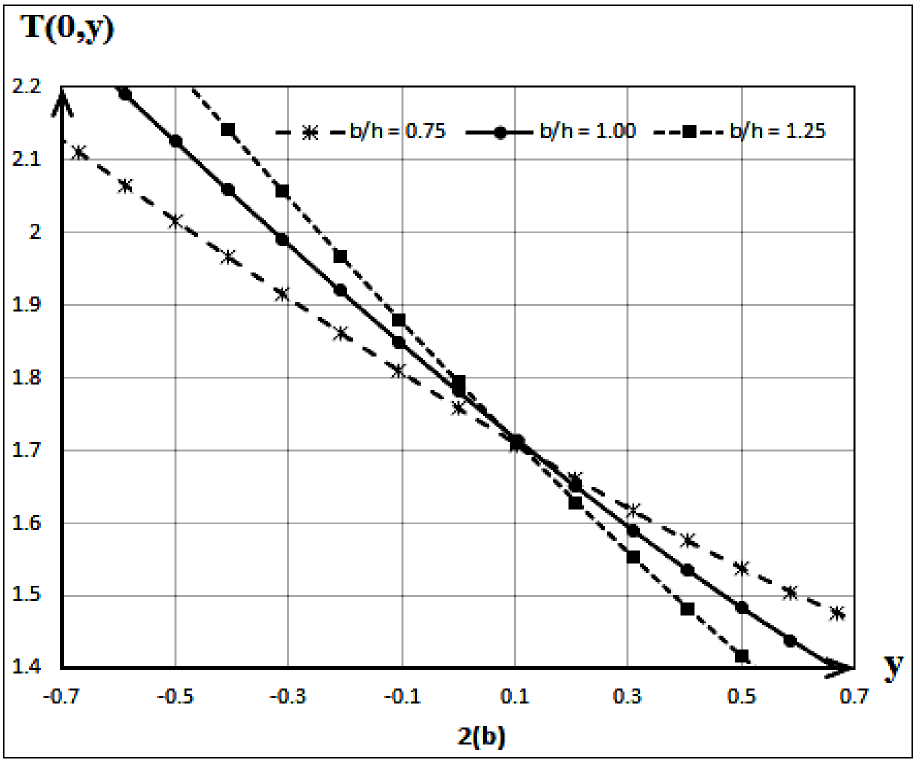

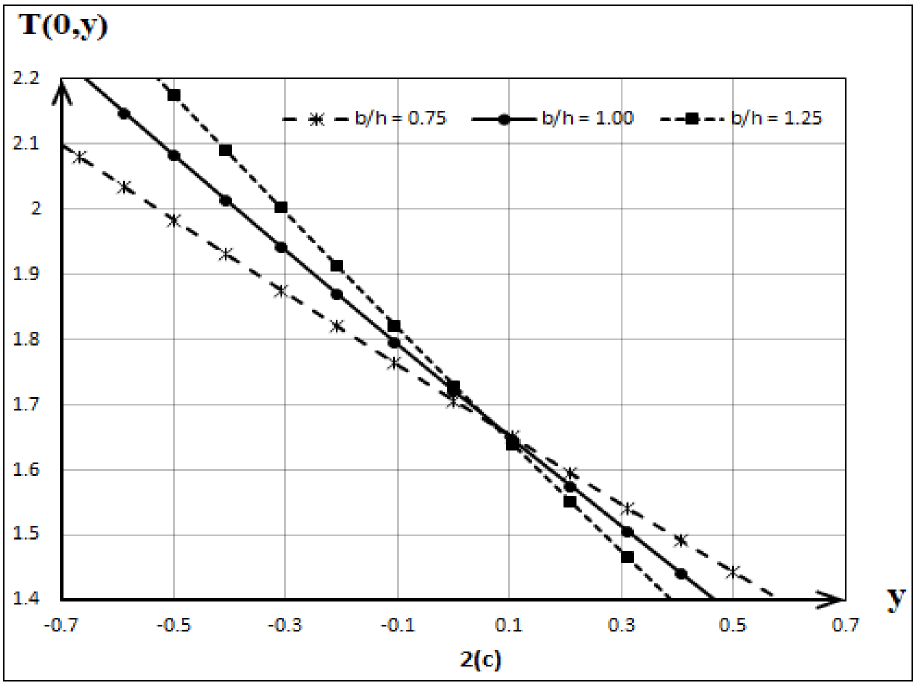

Fig 2: Temperature distribution on (a) crack face and extension line, (b) and (c) the line $x = 0$ in R_1 and R_2 respectively for different $\frac{b}{h}$ when $\delta = 0.10$, $\kappa = 1.8, H = 1.0,$ $\alpha_t = 1.5, T_1 = 2.5, T_2 = 1.0.$

Fig. 3(a), 3(b) and 3(c) depict the effects of the inhomogeneity thermal parameter δ on temperature distribution along and the vertical centerline $x = 0$ of the crack face. In Fig. 3(a) the temperature profiles are symmetric about the crack center $x = 0$, and the temperature decreases as δ increases with deeper troughs and broader central regions. In Fig. 3(b) and 3(c), we find that the temperature distribution along the vertical centerline $(x = 0)$ decreases linearly in both regions region R_1 and R_2 with increase of the inhomogeneity thermal parameter δ. Notably, temperature variations at corresponding points above and below the crack line on $x = 0$ exhibit opposite trends.

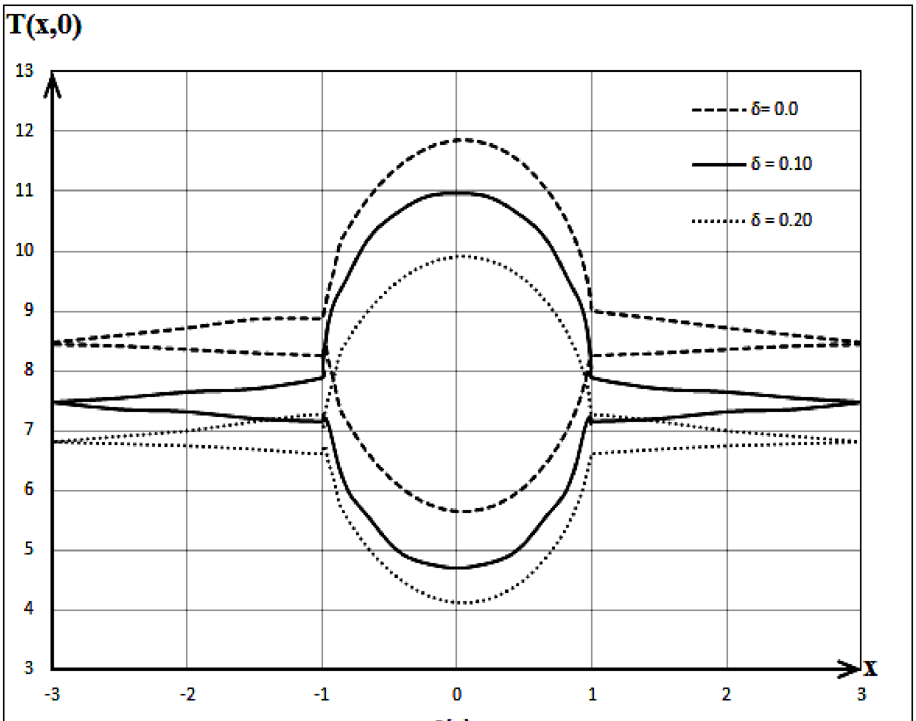
T(x,0)
13
12
11
10
9
8
7
6
5
4
3
δ= 0.0
δ = 0.10
δ = 0.20
-3
-2
-1
0
1
2
3
x

3(a)

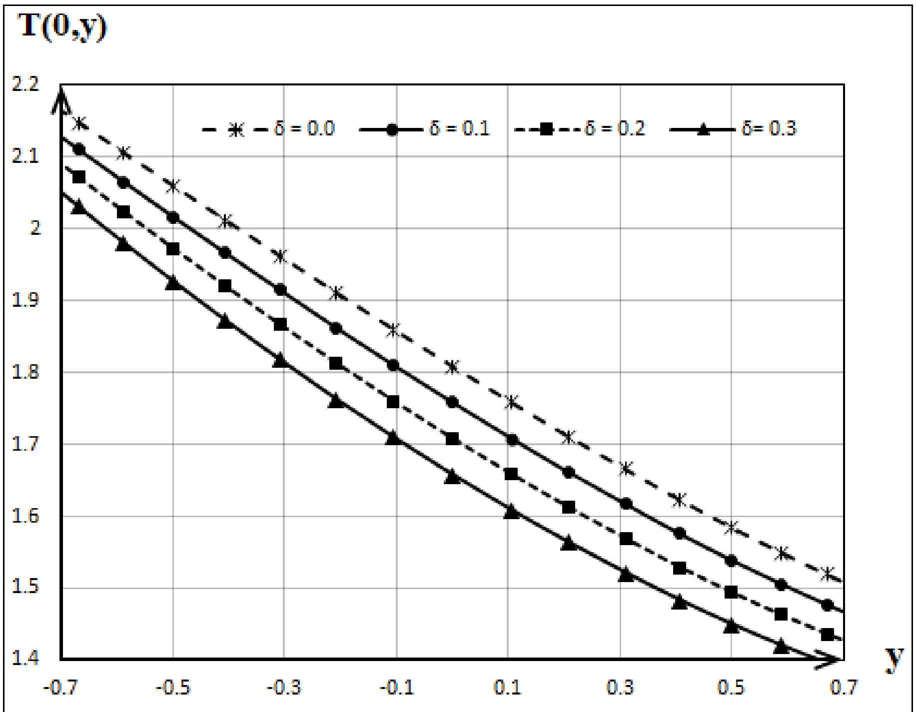
T(0,y)
δ = 0.0
δ = 0.1
δ = 0.2
δ= 0.3
2.2
2.1
2
1.9
1.8
1.7
1.6
1.5
1.4
-0.7
-0.5
-0.3
-0.1
0.1
0.3
0.5
0.7
y

3(b)

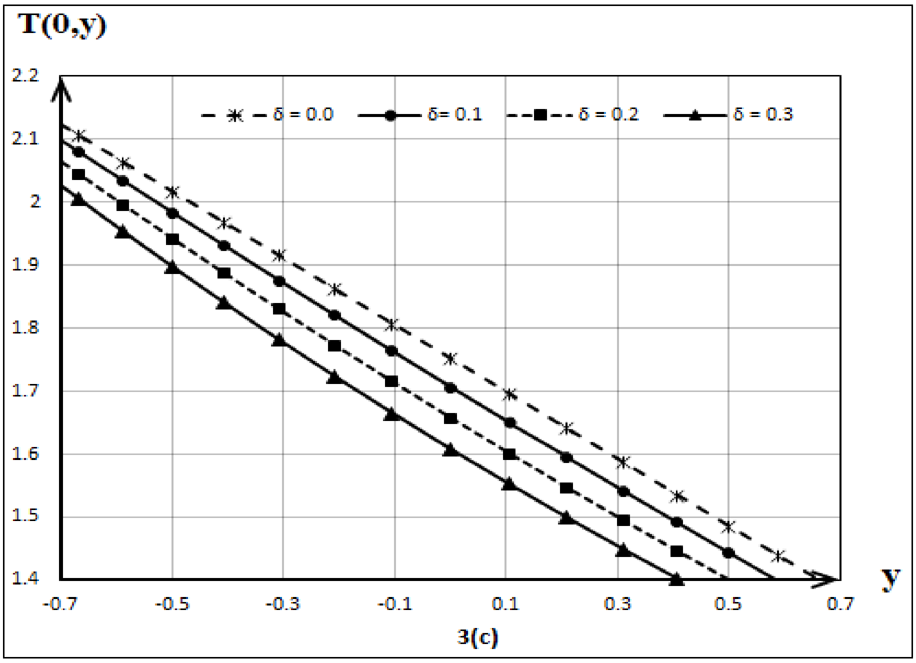

Fig.3: Effect of inhomogeneity thermal parameter δ on (a) the crack face and extension line with $\frac{b}{h} = 0.20$, (b) and (c) the line x = 0 in R_1 and R_2 respectively with $\frac{b}{h} = 0.75$ and

$$\kappa = 1.8, H = 1.0, \alpha_t = 1.5, T_1 = 2.5, T_2 = 1.0.$$

Fig. 4(a) and 4(b) illustrate the variation of the Thermo-Mechanical Stress Intensity Factor (TMSIF), denoted as $k'(b)$, with respect to the normalized crack length $\frac{b}{h}$ for different applied loads under both tensile and compressive loading conditions in region R_1 and R_2. The results confirm that the TMSIF is strongly influenced by crack length and mechanical load. A distinct critical crack size exists where the risk of failure is maximized. Tensile loading increases the severity of the stress intensity, while compressive loading reduces it. Fig. 5(a) and 5(b) reveal the influence of the inhomogeneity parameter δ on TMSIF for both tensile and compressive thermal loading cases in both regions. The graphs depict a distinct peak in TMSIF at a particular $\frac{b}{h}$ value for all δ values, indicating a critical position where the TMSIF is maximized. This peak is noticeably more pronounced under tensile thermal conditions compared to compressive ones, reflecting the greater severity of crack tip stress fields in tension. As the inhomogeneity parameter δ increases, the magnitude of the TMSIF generally increases in both cases. The graded parameter β in Fig. 6 (a) and 6(b), significantly influences the TMSIF. Higher β values lead to greater stress intensities, especially under tensile loading. The location of the peak remains largely unchanged, while the magnitude of $k'(b)$ is sensitive to β, highlighting the importance of material gradation in controlling stress distribution in thermo-mechanical environments. Fig. 7(a) and 7(b) show the variation of TMSIF with $\frac{b}{h}$ for different crack aspect ratios. The results indicate a gradual increase at low $\frac{b}{h}$, followed by a sharp peak at intermediate values, and then a rapid decline to a stable level. Tensile loading consistently yields higher TMSIF than compressive loading, particularly near the peak. Increasing $\frac{b}{h}$ enhances the peak magnitude, highlighting the strong influence of crack geometry and loading conditions on thermo-mechanical fracture behavior. Fig. 8(a) and 8(b) present the normalized crack surface displacement profiles along the crack surface for different values of the applied load Q in both the regions. The results demonstrate that the displacement distribution is symmetric with respect to the crack center, exhibiting a maximum at the mid-point and gradually reducing to zero at the crack tips. As Q increases, the displacement magnitude systematically decreases, indicating a strong influence of this parameter on crack opening behavior. Fig. 9(a) and 9(b) depict the influence of the thermal inhomogeneity parameter δ on the normalized crack surface displacement in both the regions. The profiles clearly show that the crack opening decreases progressively as δ increases. Although the peak displacement varies with δ, the symmetric parabolic nature of the distribution about the crack center is preserved, indicating that δ acts primarily as a controlling factor for the magnitude of displacement without altering the overall displacement pattern. Fig. 10(a) and 10(b) present the normalized crack surface displacement for various values of the graded material parameter β in regions R_1 and R_2, respectively. In both regions, the displacement profiles exhibit symmetry with maximum values at the crack center and vanishing at the crack tips. A clear trend is observed where increasing β results in a reduction of the crack opening, demonstrating the restraining effect of material gradation on displacement. These results emphasize that stronger gradation effectively suppresses crack surface separation, thereby enhancing the resistance of the graded structure against tensile crack opening. Fig. 11(a) and 11(b) display the normalized crack surface displacement for different values of the crack length ratio $\frac{a}{b}$ in both regions. In both cases, the displacement profiles remain symmetric, with maximum values at the crack center and tapering to zero at the tips. It is evident that an increase in $\frac{a}{b}$ reduces the overall displacement magnitude, demonstrating that longer relative crack lengths tend to suppress crack opening.

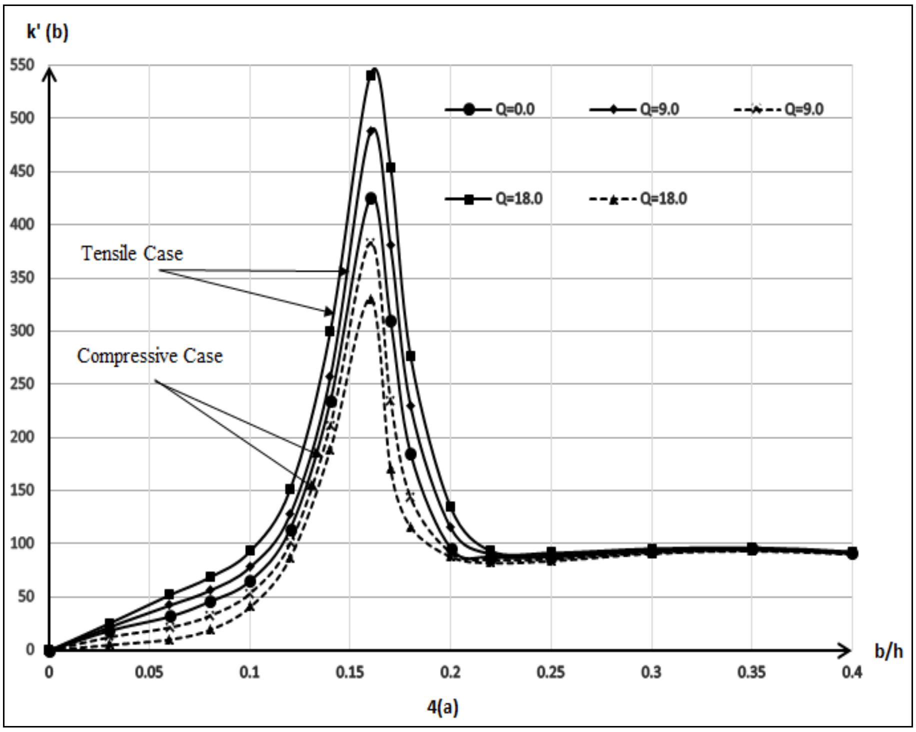

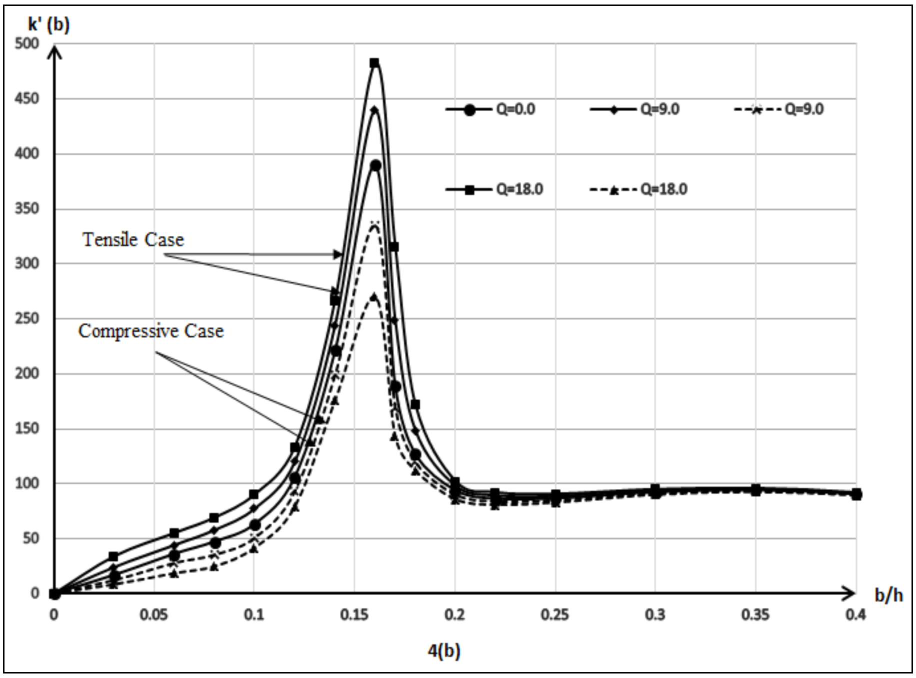

Fig 4: Variation of TMSIF with $\frac{b}{h}$ for different loads Q in both cases in (a) R_1 (b) R_2

when

$\frac{a}{b} = 0.0, \delta = 0.05, \kappa = 1.8, \beta = 0.10, H = 1.0, \alpha_t = 1.5, T_1 = 2.5, T_2 = 1.0.$

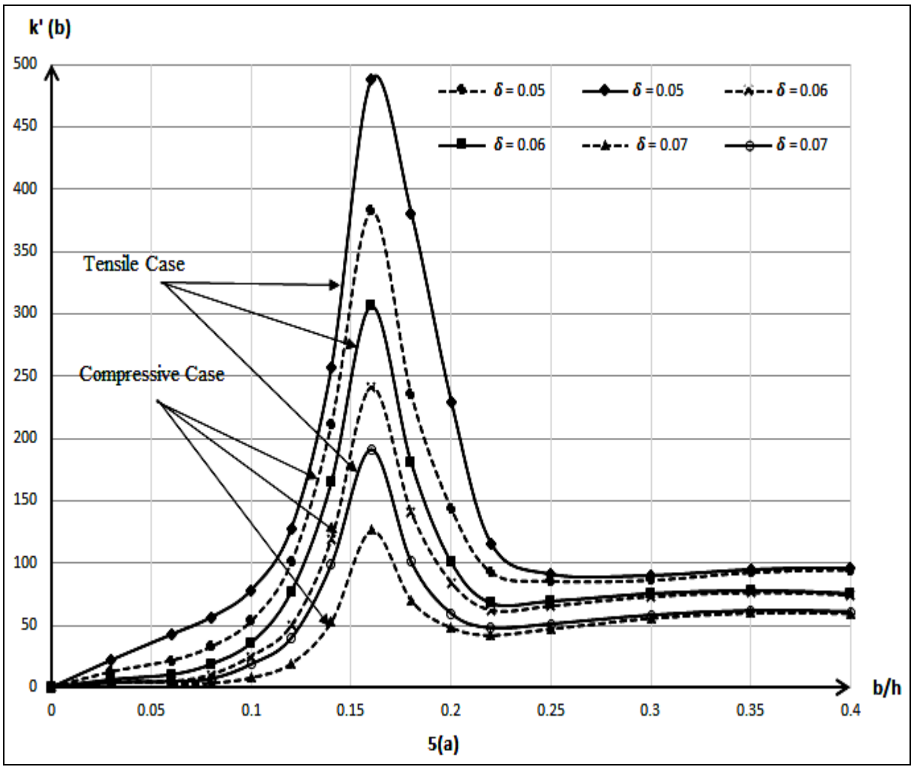

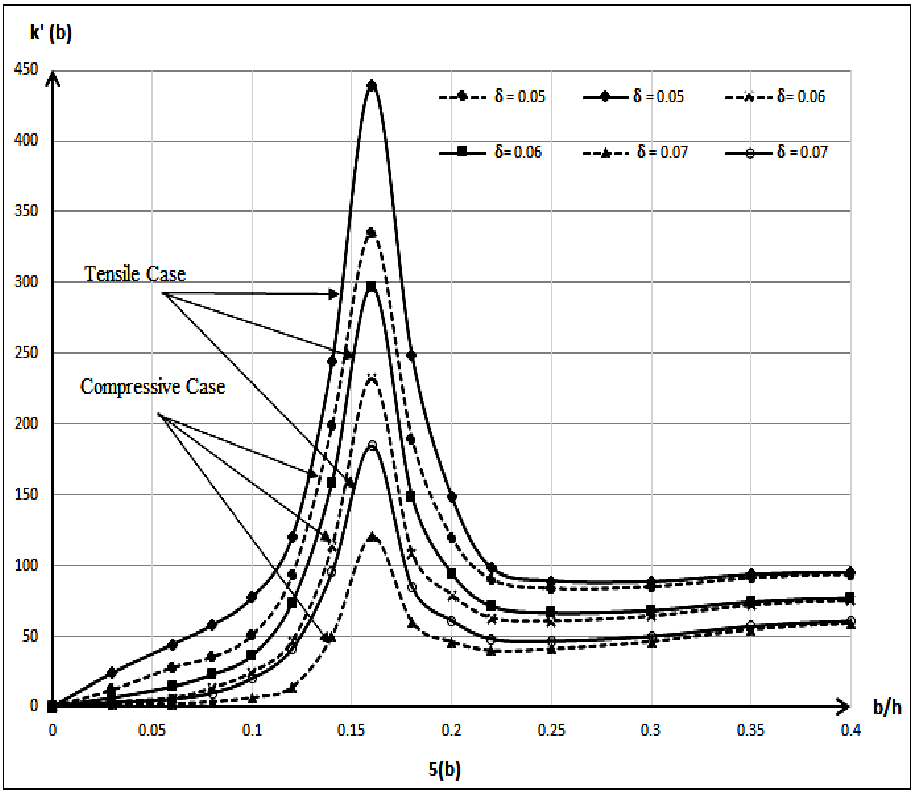

Fig 5: Effect of inhomogeneity parameter δ on TMSIF, $k'(b)$ for both cases in (a) R_1 (b) R_2 when

$\frac{a}{b} = 0.0, Q = 9.0, \kappa = 1.8, \beta = 0.10, H = 1.0, \alpha_t = 1.5, T_1 = 2.5, T_2 = 1.0.$

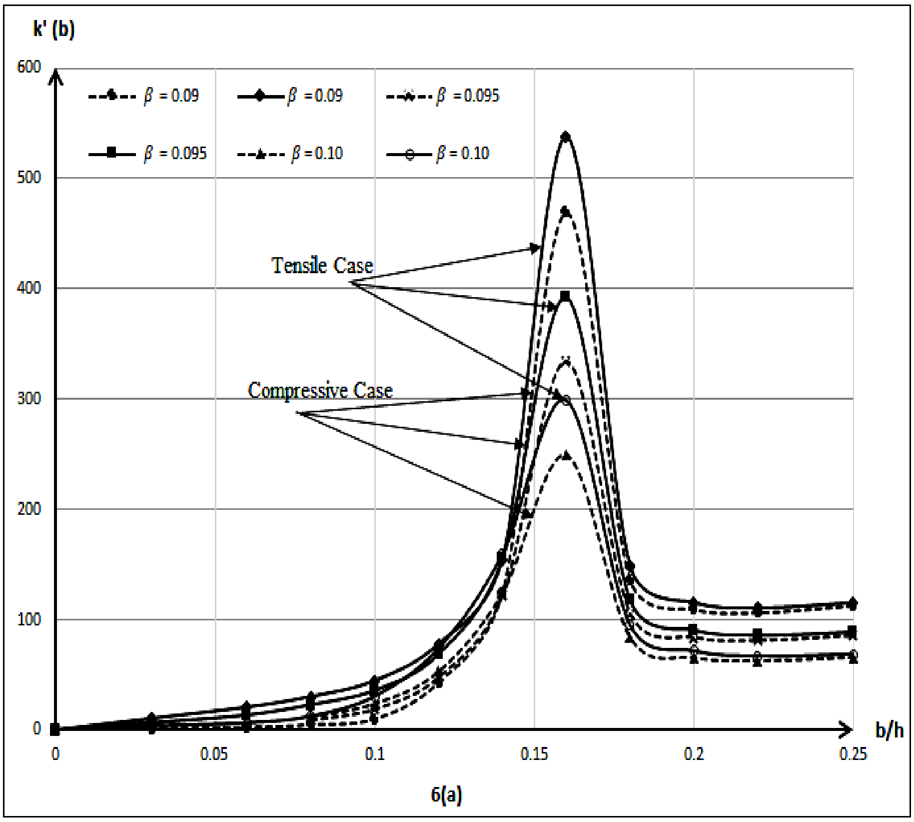

6(a)

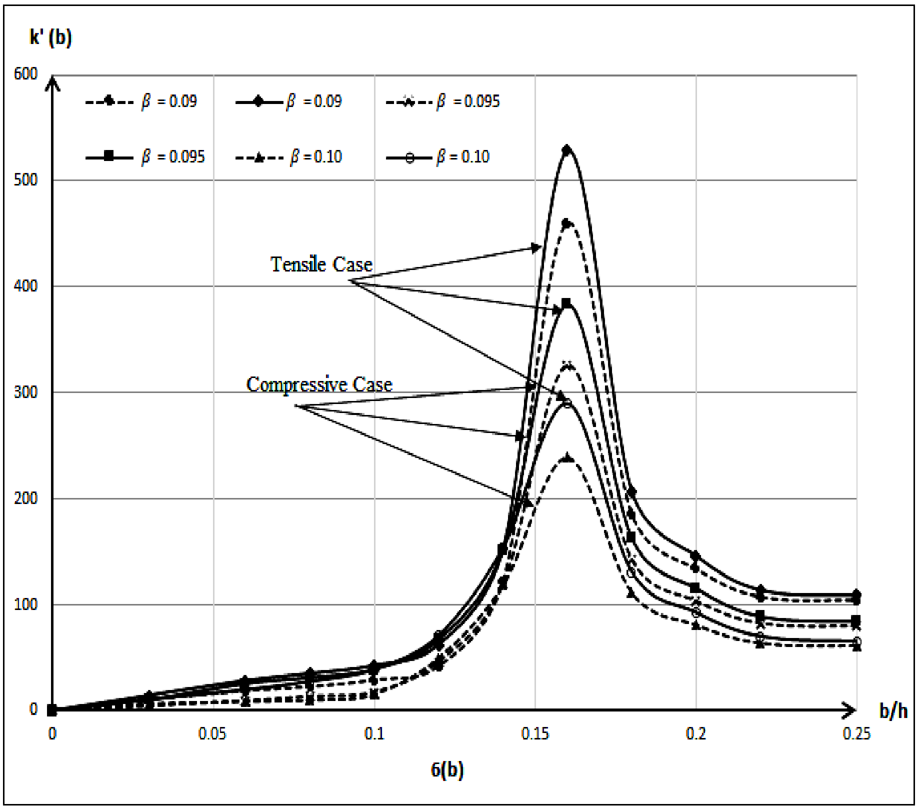

6(b)

Fig 6: Effect of graded parameter β on TMSIF, $k'(b)$ for both cases in (a) R_1 (b) R_2 when

$\frac{a}{b} = 0.0, Q = 7.0, \kappa = 1.8, \delta = 0.06, H = 1.0, \alpha_t = 1.5, T_1 = 2.5, T_2 = 1.0.$

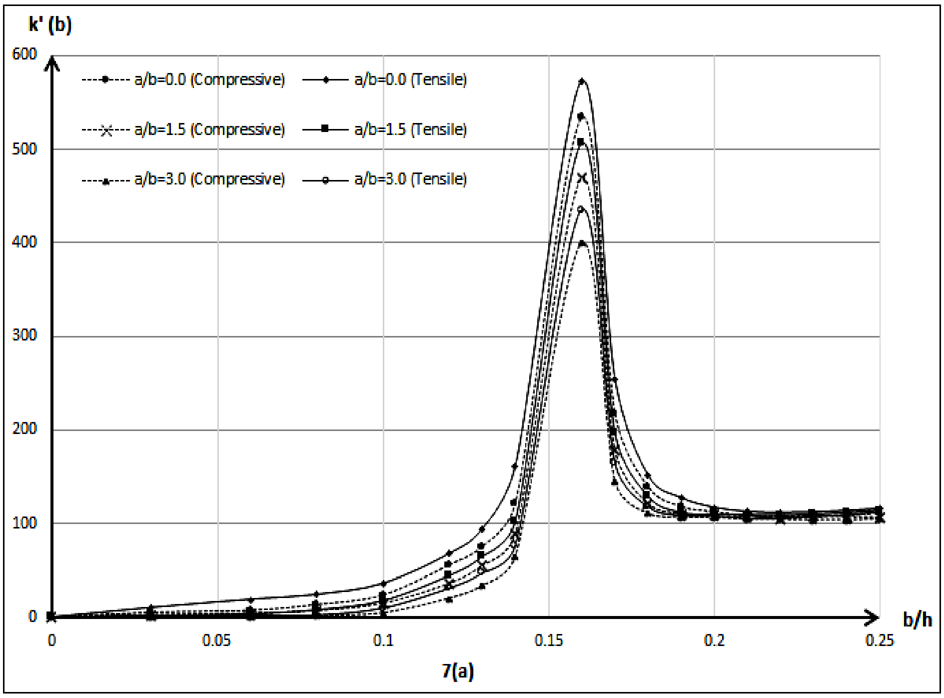

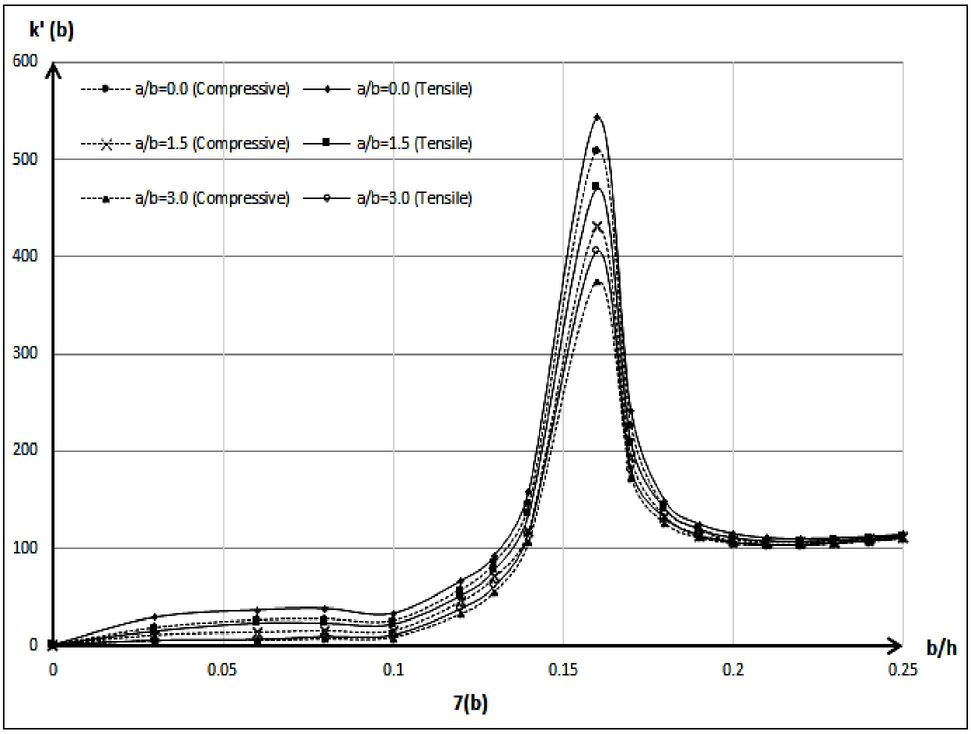

Fig 7: Variation of TMSIF, $k'(b)$ for different values $\frac{a}{b}$ for both cases in (a) R_1 (b) R_2 when

$Q = 10.0, \delta = 0.06, \kappa = 1.8, \beta = 0.09, H = 1.0, \alpha_t = 1.5, T_1 = 2.5, T_2 = 1.0.$

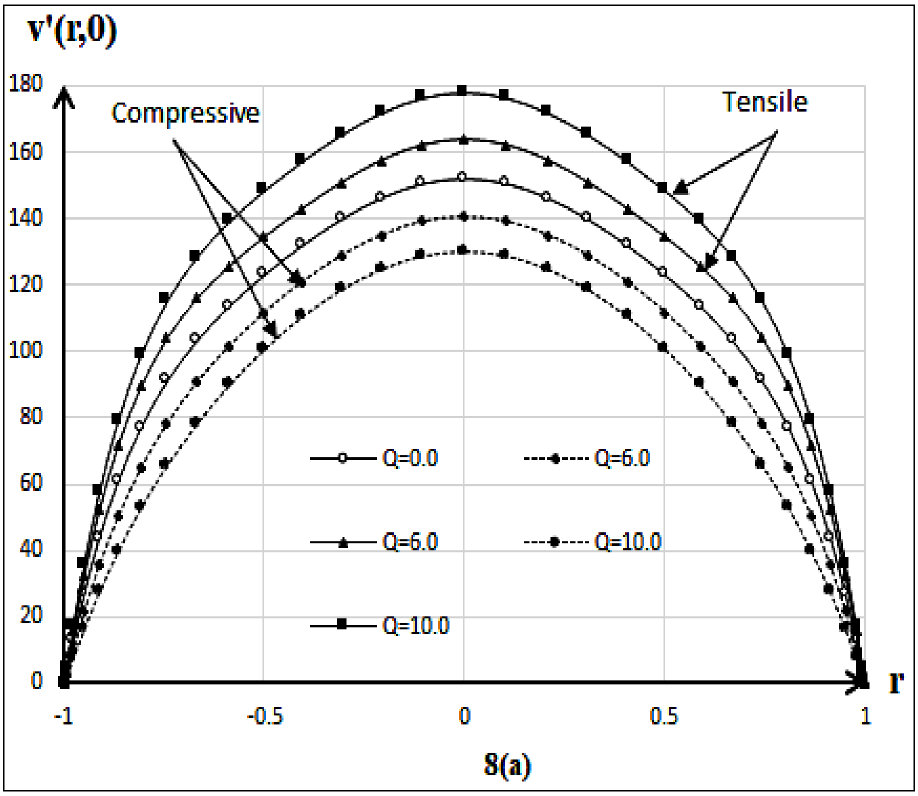

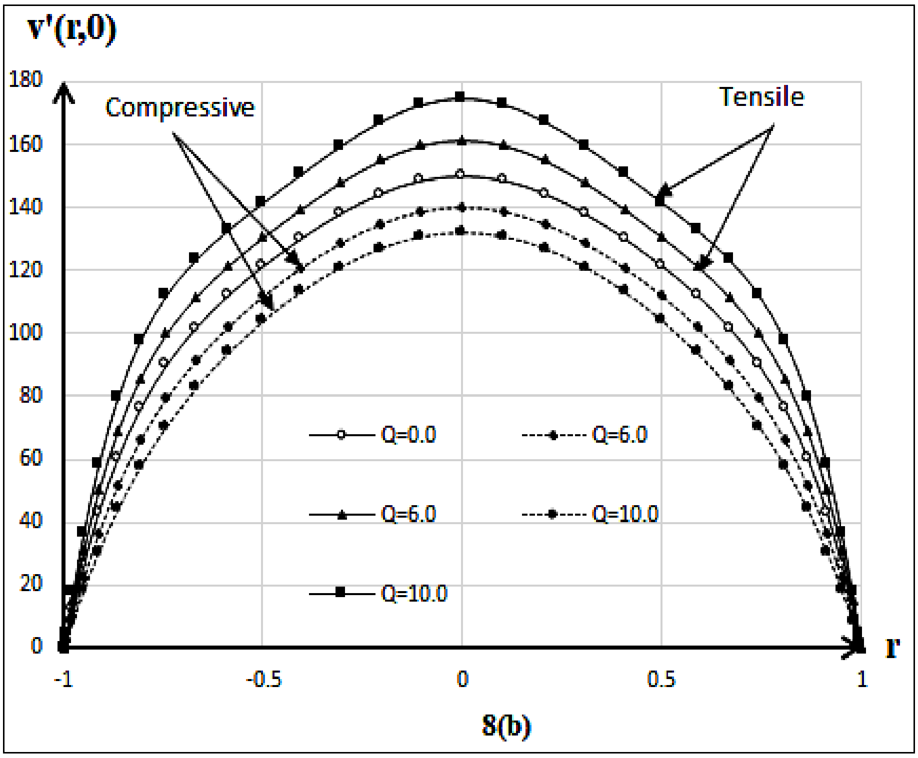

Fig 8: Normalized crack surface displacement $v'(r,0)$ for various values of Q for both cases in (a) R_1 (b) R_2 when $\frac{b}{h} = 0.25$, $\frac{a}{b} = 0.0, \delta = 0.06$, $\kappa = 1.8, \beta = 0.09, H = 1.0$, $\alpha_t = 1.5, T_1 = 2.5, T_2 = 1.0$.

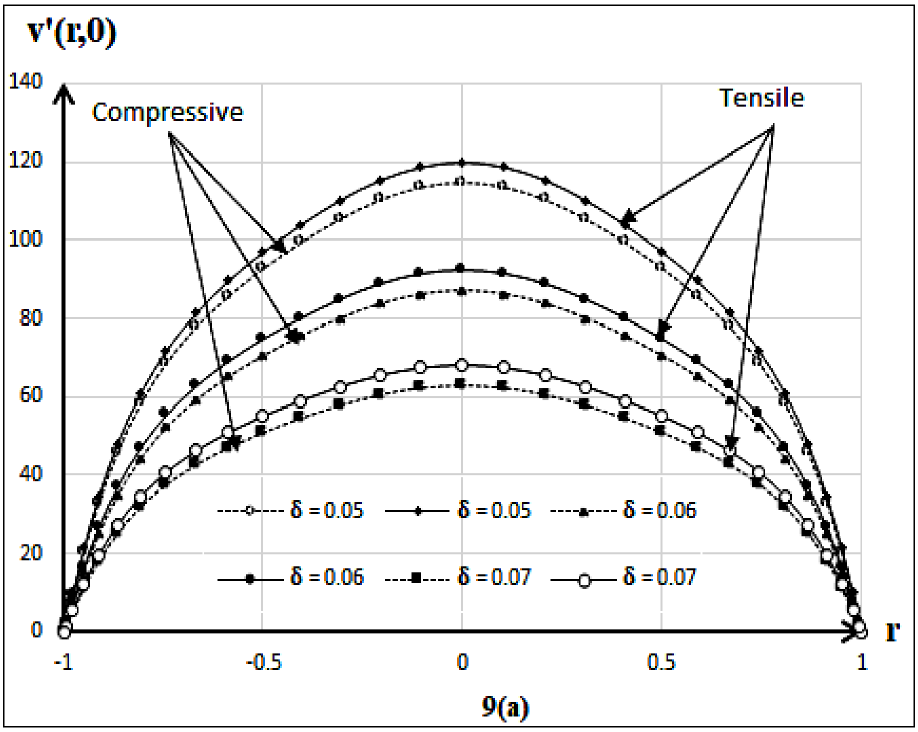

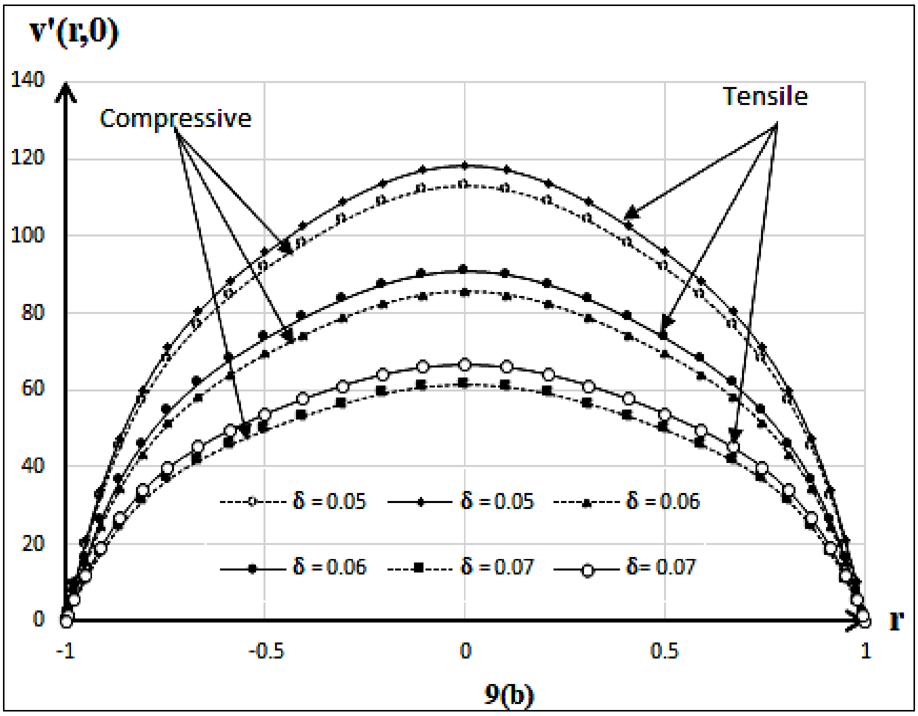

Fig 9: Normalized crack surface displacement $v'(r,0)$ for various values of δ for both cases in (a) R_1 (b) R_2 when $\frac{b}{h} = 0.25$, $\frac{a}{b} = 0.0, \kappa = 1.8, \beta = 0.10, H = 1.0,$ $Q = 9.0, \alpha_t = 1.5, T_1 = 2.5, T_2 = 1.0.$

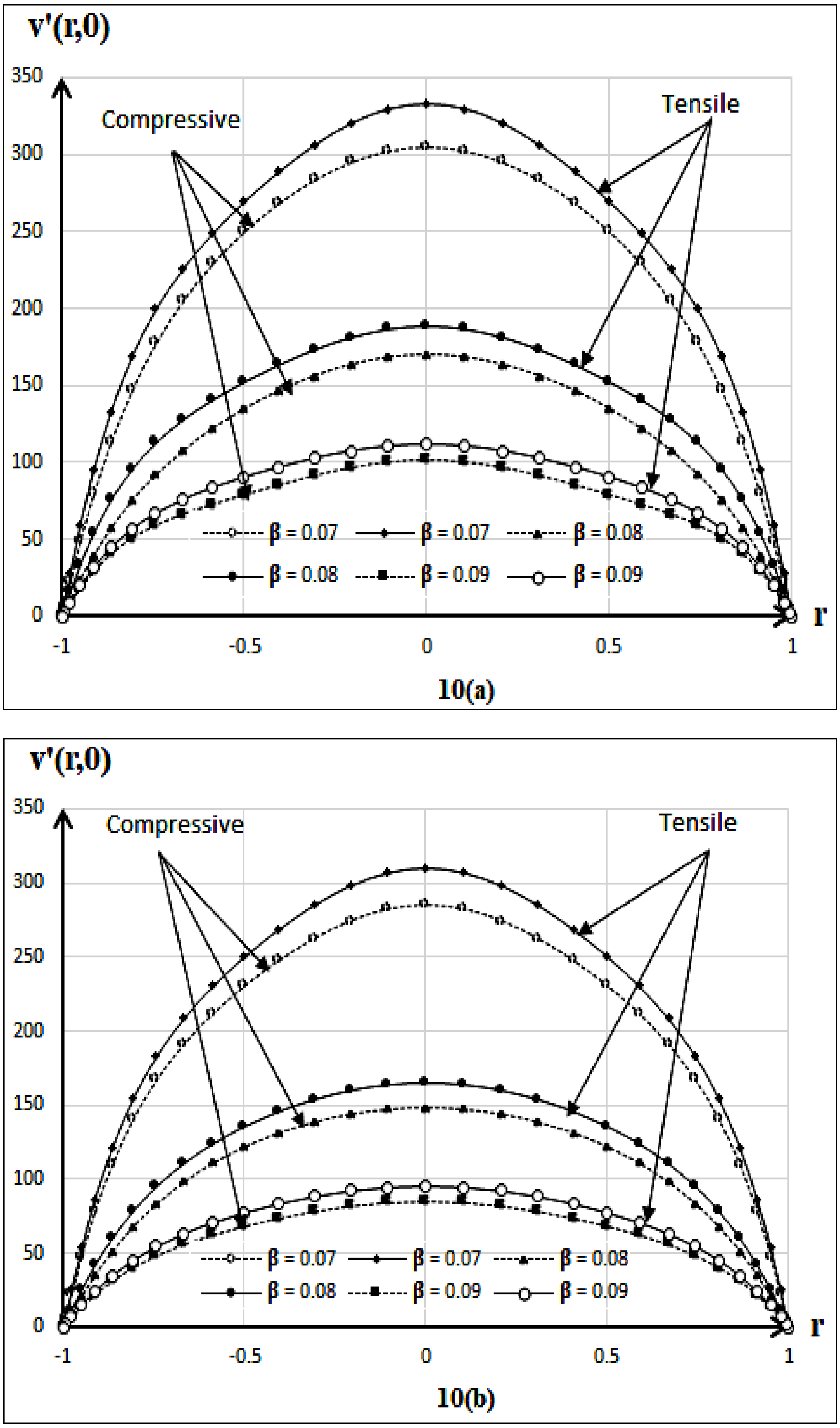

Fig 10: Normalized crack surface displacement $v'(r,0)$ for various values of β for both cases in (a) R_1 (b) R_2 when $\frac{b}{h} = 0.30$, $\frac{a}{b} = 0.0, \kappa = 1.8, \delta = 0.07, H = 1.0,$ $Q = 11.0, \alpha_t = 1.5, T_1 = 2.5, T_2 = 1.0.$

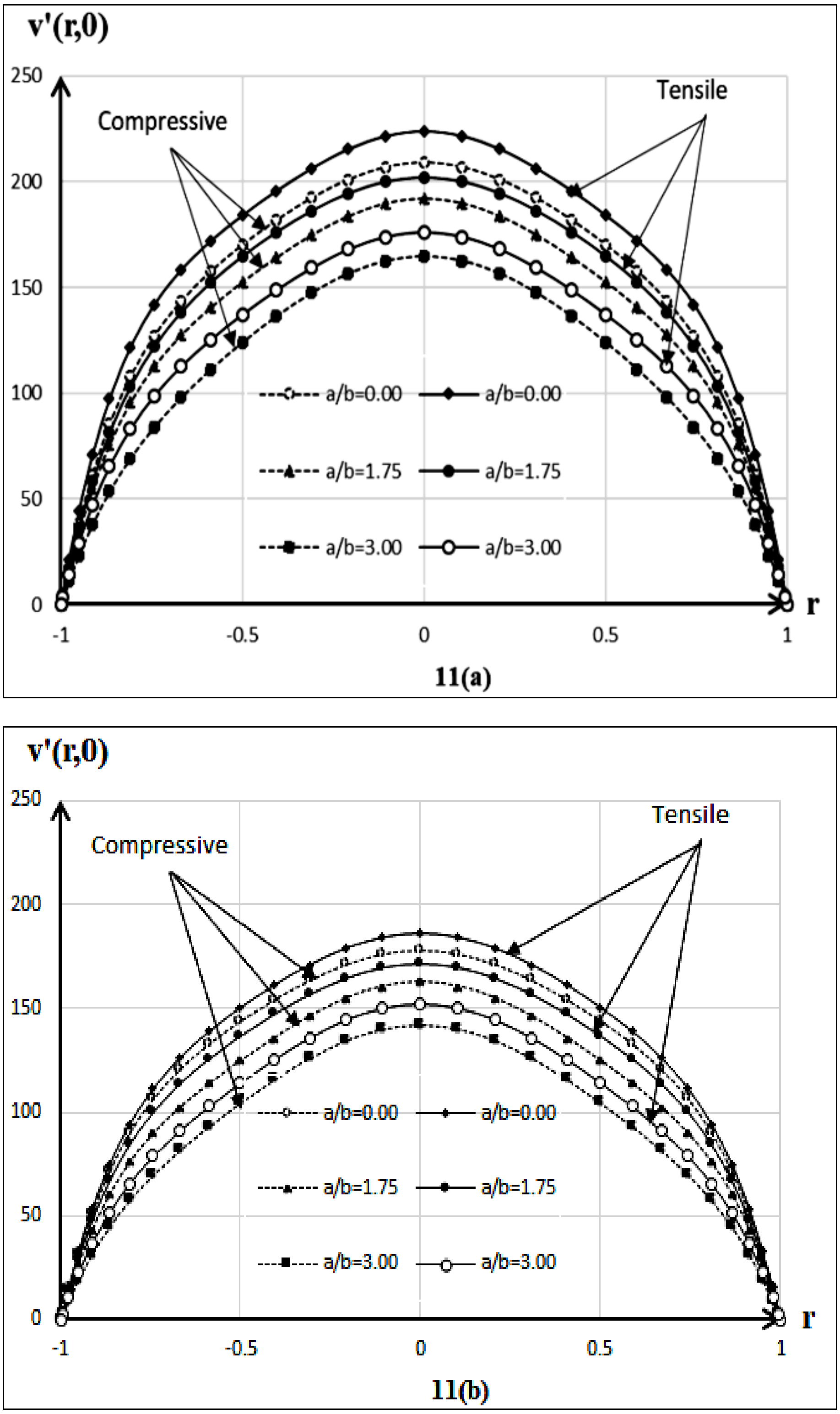

Fig 11: Normalized crack surface displacement $v'(r,0)$ for various values of $\frac{a}{b}$ for both cases in (a) R_1 (b) R_2 when

$$\frac{b}{h} = 0.30,\ \beta = 0.08, \kappa = 1.8, \delta = 0.07, H = 1.0,$$
$$Q = 11.0, \alpha_t = 1.5, T_1 = 2.5, T_2 = 1.0.$$

Fig. 12 shows the variation of SIF, TSIF, and TMSIF in regions R_1 and R_2 with respect to the normalized crack length $\frac{b}{h}$. All three factors increase gradually, peak at critical crack lengths, and then decline to a stable level. Although both regions exhibit similar trends, differences in peak values suggest the influence of material gradation and structure. TSIF remains lower than SIF due to its purely thermal origin, while TMSIF exceeds both under tensile thermal loading, highlighting the amplifying effect of combined thermal and mechanical loads. In contrast, compressive thermal loading reduces TMSIF, indicating improved structural stability.

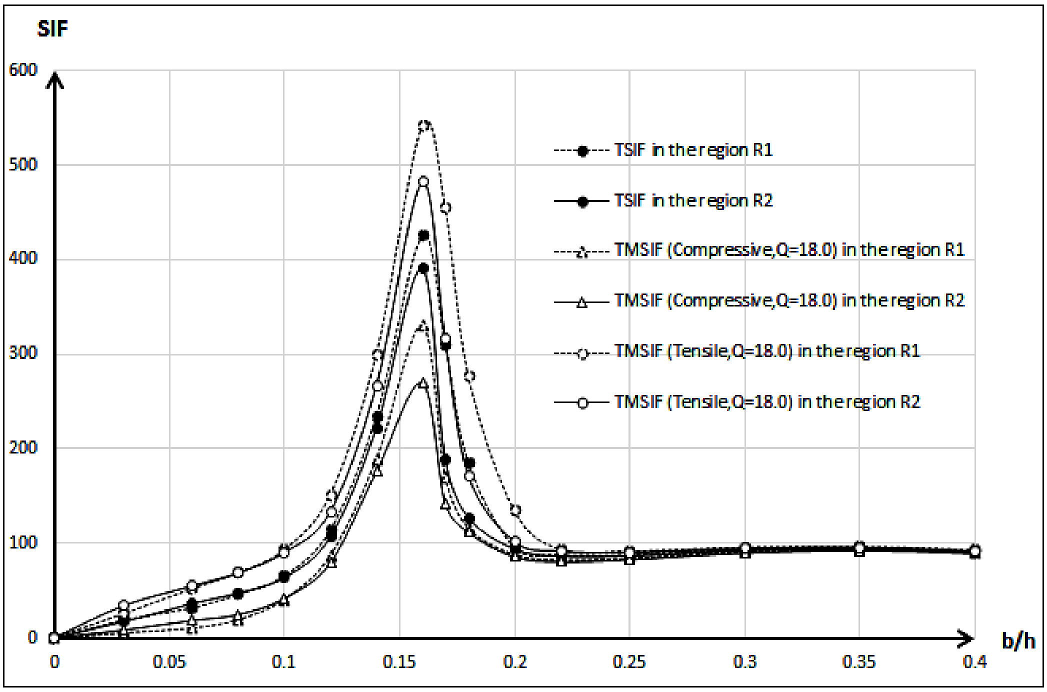

Fig 12: Comparison of TMSIF and TSIF for both the regions R_1 and R_2 when

$\frac{a}{b} = 0.0,\ \beta = 0.10, \kappa = 1.8, \delta = 0.05, H = 1.0, \alpha_t = 1.5, T_1 = 2.5, T_2 = 1.0.$

8. Conclusion

These findings offer valuable guidance for applying functionally graded materials in high-temperature environments like aerospace, nuclear, or thermal barrier systems. Tensile thermal stresses can accelerate crack growth and reduce durability, while compressive thermal fields help suppress cracks and enhance longevity. Thus, tailoring thermal gradients and stress distributions is key to improving fracture resistance

References

1. Nowacki W. Thermoelasticity. London: Pergamon Press; 1962.
2. Nowinski JL. Theory of Thermoelasticity with Applications. Alphen Aan Den Rijn: Sijthoff and Noordhoff International Publishers; 1978.
3. Boley BA, Weiner JH. Theory of Thermal Stresses. New York: Dover Publications; 2012.
4. Dag S, Kadioglu S, Yahsi OS. Circumferential crack problem for an FGM cylinder under thermal stresses. Journal of Thermal Stresses. 1999; 22:659-687.
5. Dag S, Erdogan F. A surface crack in a graded medium under general loading conditions. Journal of Applied Mechanics. 2002; 69:580-588.
6. Sherief HH, El-Mahraby NM. An internal penny-shaped crack in an infinite thermoelastic solid. Journal of Thermal Stresses. 2003; 26:333-352.
7. Chaudhuri PK, Ray S. Sudden twisting of a penny-shaped crack in a nonhomogeneous elastic medium. Journal of Mathematical and Physical Sciences. 1995; 29:207-221.
8. Chaudhuri PK, Ray S. Thermal stress in a nonhomogeneous transversely isotropic medium containing a penny-shaped crack. Bulletin of the Calcutta Mathematical Society. 2006;98(6):547-570.
9. Patra R, Barik SP, Kundu M, Chaudhuri PK. Plane elastostatic solution in an infinite functionally graded layer weakened by a crack lying in the middle of the layer. International Journal of Computational Mathematics. 2014; 2014:1-9. Article ID 358617.
10. Patra R, Barik SP, Chaudhuri PK. Steady-state thermoelastic problem in an infinite elastic layer weakened by a crack lying in the middle of the layer. International Journal of Engineering Science Invention. 2016;5(10):21-36.
11. Patra R, Barik SP, Chaudhuri PK. An internal crack problem in an infinite transversely isotropic elastic layer. International Journal of Advances in Applied Mathematics and Mechanics. 2015;3(1):62-70.
12. Rokhi MM, Shariati M. Coupled thermoelasticity of a functionally graded cracked layer under thermomechanical shocks. Archives of Mechanics. 2013;65(2):71-96.
13. Eskandari H. Edge crack studies in rotating FGM disks. Journal of Solid Mechanics. 2016;8(3):530-539.
14. Lee DS. The problem of internal cracks in an infinite strip having a circular hole. Acta Mechanica. 2004; 169:101-110.

15. Kanaun SK. Fast solution of the elasticity problem for a planar crack of arbitrary shape in a 3D anisotropic medium. International Journal of Engineering Science. 2009;47(2):284-293. doi: 10.1016/j.ijengsci.2008.07.009
16. Barik SP, Kanoria M, Chaudhuri PK. Steady-state thermoelastic problem in an infinite functionally graded solid with a crack. International Journal of Advances in Applied Mathematics and Mechanics. 2010; 6:44-66.
17. Birinci A, Birinci F, Cakiroglu FL, Erdol R. An internal crack problem for an infinite elastic layer. Archive of Applied Mechanics. 2010;80(9):997-1005. doi:10.1007/s00419-009-0355-5
18. Rekik M, Neifar M, El-Borgi S. An axisymmetric problem of an embedded crack in a graded layer bonded to a homogeneous half-space. International Journal of Solids and Structures. 2010; 47:2043-2055.
19. Chen ZT, Hu KQ. Hyperbolic heat conduction in a cracked thermoelastic half-plane bonded to a coating. International Journal of Thermophysics. 2012;33(5):895-912. doi:10.1007/s10765-012-1190-4
20. Chang DM, Wang BL. Transient thermal fracture and crack growth behavior in brittle media based on non-Fourier heat conduction. Engineering Fracture Mechanics. 2012;94(2):29-36. doi:1 0.1016/j.engfracmech.2012.06.021
21. Markov A, Kanaun S. An efficient homogenization method for elastic media with multiple cracks. International Journal of Engineering Science. 2014; 82:205-221. doi: 10.1016/j.ijengsci.2014.05.016
22. Ding SH, Zhou YT, Xing L. Interface crack problem in layered orthotropic materials under thermo-mechanical loading. International Journal of Solids and Structures. 2014; 51:4221-4229.
23. Wang X, Zhou K, Wu MS. Interface cracks with surface elasticity in anisotropic bimaterials. International Journal of Solids and Structures. 2015; 59:110-120. doi: 10.1016/j.ijsolstr.2015.01.023
24. Ding SH, Xing L. Thermoelastic analysis of nonhomogeneous structural materials with an interface crack under uniform heat flow. Applied Mathematics and Computation. 2015; 271:22-33.
25. Lee KY, Park SJ. Thermal stress intensity factors for partially insulated interface crack under uniform heat flow. Transactions of the Korean Society of Mechanical Engineers. 1994;18(7):1705-1712.
26. Itou S. Thermal stress intensity factors of an infinite orthotropic layer with a crack. International Journal of Fracture. 2000;103(3):279-291. doi:10.1023/A:1007630808737
27. Liu L, Kardomateas GA. Thermal stress intensity factors for a crack in an anisotropic half-plane. International Journal of Solids and Structures. 2005;42(18):5208-5223. doi: 10.1016/j.ijsolstr.2005.02.025
28. Tehrani PH, Eslami MR. Analysis of thermoelastic crack problems using Green-Lindsay theory. Journal of Thermal Stresses. 2006;29(4):317-330. doi:10.1080/01495730500360484
29. Nabavi SM, Shahani AR. Thermal stress intensity factors for a cracked cylinder under transient thermal loading. International Journal of Pressure Vessels and Piping. 2009;86(2):153-163. doi: 10.1016/j.ijpvp.2008.11.024
30. Sur A, Kanoria M. Analysis of thermoelastic response in a functionally graded infinite space subjected to a Mode-I crack. International Journal of Advanced Applied Mathematics and Mechanics. 2015;3(2):33-44.
31. Hu KQ, Chen ZT. Thermoelastic analysis of a partially insulated crack in a strip under thermal impact loading using the hyperbolic heat conduction theory. International Journal of Engineering Science. 2012; 51:144-160. doi: 10.1016/j.ijengsci.2011.10.009
32. Carslaw HS, Jaeger JC. Conduction of Heat in Solids. Oxford: Clarendon Press, Oxford Science Publications; 1990.
33. Erdogan F, Gupta DS. On the numerical solution of singular integral equations. Quarterly of Applied Mathematics. 1972; 29:525-534.
34. Krenk S. On the use of the interpolation polynomial for solutions of singular integral equations. Quarterly of Applied Mathematics. 1975; 32:479-484. doi:10.1090/qam/474919
35. Gupta GD, Erdogan F. The problem of edge cracks in an infinite strip. Journal of Applied Mechanics. 1974;41(4):1001-1006.

Appendix

The expressions for $D_{ki}(\xi)$ $(k = 1,2,3$ and $i = 1, \dots\dots, 4)$ are as follows:

$$D_{11}(\xi) = \frac{1}{|L|}\left[e^{t_2 h}\{t_4 G_2 G_3 - t_3 G_2 G_4\} + e^{t_3 h}\{t_2 G_3 G_4 - t_4 G_2 G_3\} + e^{t_4 h}\{t_3 G_2 G_4 - t_2 G_3 G_4\}\right],$$

$$D_{12}(\xi) = \frac{1}{|L|}\left[e^{t_1 h}\{t_3 G_1 G_4 - t_4 G_1 G_3\} + e^{t_3 h}\{t_4 G_1 G_3 - t_1 G_3 G_4\} + e^{t_4 h}\{t_1 G_3 G_4 - t_3 G_1 G_4\}\right],$$

$$D_{13}(\xi) = \frac{1}{|L|}\left[e^{t_1 h}\{t_4 G_1 G_2 - t_2 G_1 G_4\} + e^{t_2 h}\{t_1 G_2 G_4 - t_4 G_1 G_2\} + e^{t_4 h}\{t_2 G_1 G_4 - t_1 G_2 G_4\}\right],$$

$$D_{14}(\xi) = \frac{1}{|L|}\left[e^{t_1 h}\{t_2 G_1 G_3 - t_3 G_1 G_2\} + e^{t_2 h}\{t_3 G_1 G_2 - t_1 G_2 G_3\} + e^{t_3 h}\{t_1 G_2 G_3 - t_2 G_1 G_3\}\right],$$

$D_{21}(\xi) = \frac{1}{|L|}\left[e^{(t_2+t_4)h}\{G_3G_4S_2 - G_2G_3S_4\} +\right.$
$e^{(t_3+t_4)h}\{G_2G_3S_4 - G_2G_4S_3\}$

$\left.+e^{(t_2+t_3)h}\{G_2G_4S_3 - G_3G_4S_2\}\right],$
$D_{22}(\xi) = \frac{1}{|L|}\left[e^{(t_1+t_4)h}\{G_1G_3S_4 - G_3G_4S_1\} +\right.$
$e^{(t_3+t_4)h}\{G_1G_4S_3 - G_1G_3S_4\}$

$\left.+e^{(t_1+t_3)h}\{G_3G_4S_1 - G_1G_4S_3\}\right],$

$D_{23}(\xi) = \frac{1}{|L|}\left[e^{(t_1+t_4)h}\{G_2G_4S_1 - G_1G_2S_4\} +\right.$
$e^{(t_2+t_4)h}\{G_1G_2S_4 - G_1G_4S_2\}$

$\left.+e^{(t_1+t_2)h}\{G_1G_4S_2 - G_2G_4S_1\}\right],$

$D_{24}(\xi) = \frac{1}{|L|}\left[e^{(t_1+t_3)h}\{G_1G_2S_3 - G_2G_3S_1\} +\right.$
$e^{(t_2+t_3)h}\{G_1G_3S_2 - G_1G_2S_3\}$

$\left.+e^{(t_1+t_2)h}\{G_2G_3S_1 - G_1G_3S_2\}\right],$

$D_{31}(\xi) = \frac{1}{|L|}\left[e^{t_2h}\{t_4P_2S_2G_3 + t_4P_1G_2G_3 -\right.$
$t_3P_2S_2G_4 - t_3P_1G_2G_4\}$

$+e^{t_3h}\{-t_4P_2S_3G_2 - t_4P_1G_2G_3 + t_2P_2S_3G_4 +$
$t_2P_1G_3G_4\}$

$+e^{t_4h}\{t_3P_2S_4G_2 - t_2P_2S_4G_3 + t_3P_1G_2G_4 -$
$t_2P_1G_3G_4\}$

$+e^{(t_2+t_3)h}\{t_4P_4S_3G_2 - t_4P_4S_2G_3 + P_3S_3G_2G_4 -$
$P_4S_3G_2G_4 - P_3S_2G_3G_4 + P_4S_2G_3G_4\}$

$+e^{(t_2+t_4)h}\{-t_3P_4S_4G_2 - P_3S_4G_2G_3 + P_4S_4G_2G_3 +$
$t_3P_4S_2G_4 + P_3S_2G_3G_4 - P_4S_2G_3G_4\}$

$+e^{(t_3+t_4)h}\{t_2P_4S_4G_3 + P_3S_4G_2G_3 - P_4S_4G_2G_3 -$
$\left.t_2P_4S_3G_4 - P_3S_3G_2G_4 + P_4S_3G_2G_4\}\right],$

$D_{32}(\xi) = \frac{1}{|L|}\left[e^{t_1h}\{-t_4P_2S_1G_3 - t_4P_1G_1G_3 +\right.$
$t_3P_2S_1G_4 + t_3P_1G_1G_4\}$

$+e^{t_3h}\{t_4P_2S_3G_1 + t_4P_1G_1G_3 - t_1P_2S_3G_4 -$
$t_1P_1G_3G_4\}$

$+e^{t_4h}\{-t_3P_2S_4G_1+t_1P_2S_4G_3-t_3P_1G_1G_4+$
$t_1P_1G_3G_4\}$

$+e^{(t_1+t_3)h}\{-t_4P_4S_3G_1+t_4P_4S_1G_3-P_3S_3G_1G_4+$
$P_4S_3G_1G_4+P_3S_1G_3G_4-P_4S_1G_3G_4\}$

$+e^{(t_1+t_4)h}\{t_3P_4S_4G_1+P_3S_4G_1G_3-P_4S_4G_1G_3-$
$t_3P_4S_1G_4-P_3S_1G_3G_4+P_4S_1G_3G_4\}$

$+e^{(t_3+t_4)h}\{-t_4P_4S_4G_3-P_3S_4G_1G_3+P_4S_4G_1G_3+$
$t_1P_4S_3G_4+P_3S_3G_1G_4-P_4S_3G_1G_4\}]$,

$D_{33}(\xi)=\frac{1}{|L|}\left[e^{t_1h}\{t_4P_2S_1G_2+t_4P_1G_1G_2-\right.$
$t_2P_2S_1G_4-t_2P_1G_1G_4\}$

$+e^{t_2h}\{-t_4P_2S_2G_1-t_4P_1G_1G_2+t_1P_2S_2G_4+$
$t_1P_1G_2G_4\}$

$+e^{t_4h}\{t_2P_2S_4G_1-t_1P_2S_4G_2+t_2P_1G_1G_4-$
$t_1P_1G_2G_4\}$

$+e^{(t_1+t_2)h}\{t_4P_4S_2G_1-t_4P_4S_1G_2+P_3S_2G_1G_4-P_4S_2G_1G_4-P_3S_1G_2G_4+P_4S_1G_2G_4\}$

$+e^{(t_1+t_4)h}\{-t_2P_4S_4G_1-P_3S_4G_1G_2+P_4S_4G_1G_2+$
$t_2P_4S_1G_4+P_3S_1G_2G_4-P_4S_1G_2G_4\}$

$+e^{(t_2+t_4)h}\{t_1P_4S_4G_2+P_3S_4G_1G_2-P_4S_4G_1G_2-t_1P_4S_2G_4-P_3S_2G_1G_4+P_4S_2G_1G_4\}]$,

$D_{34}(\xi)=\frac{1}{|L|}\left[e^{t_1h}\{-t_3P_2S_1G_2-t_3P_1G_1G_2+\right.$
$t_2P_2S_1G_3+t_2P_1G_1G_3\}$

$+e^{t_2h}\{t_3P_2S_2G_1+t_3P_1G_1G_2-t_1P_2S_2G_3-$
$t_1P_1G_2G_3\}$

$+e^{t_3h}\{-t_2P_2S_3G_1+t_1P_2S_3G_2-t_2P_1G_1G_3+$
$t_1P_1G_2G_3\}$

$+e^{(t_1+t_2)h}\{-t_3P_4S_2G_1+t_3P_4S_1G_2-P_3S_2G_1G_3+P_4S_2G_1G_3+P_3S_1G_2G_3-P_4S_1G_2G_3\}$

$+e^{(t_1+t_3)h}\{t_2P_4S_3G_1+P_3S_3G_1G_2-P_4S_3G_1G_2-$
$t_2P_4S_1G_3-P_3S_1G_2G_3+P_4S_1G_2G_3\}$

$+e^{(t_2+t_3)h}\{-t_1P_4S_3G_2-P_3S_3G_1G_2+P_4S_3G_1G_2+t_1P_4S_2G_3+P_3S_2G_1G_3-P_4S_2G_1G_3\}]$.